ACS MEASUREMENT SCIENCE Au
AN OPEN ACCESS JOURNAL OF THE AMERICAN CHEMICAL SOCIETY

pubs.acs.org/measureau

Article

Probing Individual Particles Generated at the Freshwater–Seawater Interface through Combined Raman, Photothermal Infrared, and X-ray Spectroscopic Characterization

Jessica A. Mirrielees, Rachel M. Kirpes, Savannah M. Haas, Carlton D. Rauschenberg, Patricia A. Matrai, Allison Remenapp, Vanessa L. Boschi, Amanda M. Grannas, Kerri A. Pratt,* and Andrew P. Ault*

Cite This: *ACS Meas. Sci. Au* 2022, 2, 605–619

Read Online

ACCESS | Metrics & More | Article Recommendations | Supporting Information

ABSTRACT: Sea spray aerosol (SSA) is one of the largest global sources of atmospheric aerosol, but little is known about SSA generated in coastal regions with salinity gradients near estuaries and river outflows. SSA particles are chemically complex with substantial particle-to-particle variability due to changes in water temperature, salinity, and biological activity. In previous studies, the ability to resolve the aerosol composition to the level of individual particles has proven necessary for the accurate parameterization of the direct and indirect aerosol effects; therefore, measurements of individual SSA particles are needed for the characterization of this large source of atmospheric aerosol. An integrated analytical measurement approach is required to probe the chemical composition of individual SSA particles. By combining complementary vibrational microspectroscopic (Raman and optical photothermal infrared, O-PTIR) measurements with elemental information from computer-controlled scanning electron microscopy with energy-dispersive X-ray analysis (CCSEM–EDX), we gained unique insights into the individual particle chemical composition and morphology. Herein, we analyzed particles from four experiments on laboratory-based SSA production using coastal seawater collected in January 2018 from the Gulf of Maine. Individual salt particles were enriched in organics compared to that in natural seawater, both with and without added microalgal filtrate, with greater enrichment observed for smaller particle sizes, as evidenced by higher carbon/sodium ratios. Functional group analysis was carried out using the Raman and infrared spectra collected from individual SSA particles. Additionally, the Raman spectra were compared with a library of Raman spectra consisting of marine-derived organic compounds. Saccharides, followed by fatty acids, were the dominant components of the organic coatings surrounding the salt cores of these particles. This combined Raman, infrared, and X-ray spectroscopic approach will enable further understanding of the factors determining the individual particle composition, which is important for understanding the impacts of SSA produced within estuaries and river outflows, as well as areas of snow and ice melt.

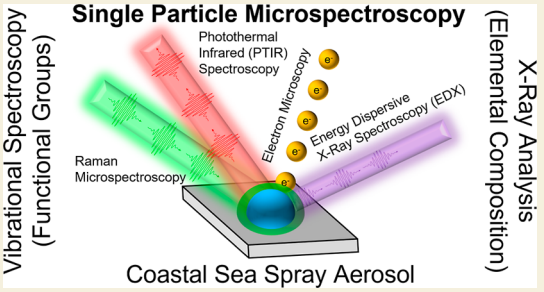

KEYWORDS: *sea spray aerosol, individual particle analysis, computer-controlled X-ray spectroscopy, Raman microspectroscopy, optical photothermal infrared spectroscopy*

INTRODUCTION

Sea spray aerosol (SSA) contributes the largest global flux of aerosol to the troposphere.[1] SSA is produced via seawater wave breaking, which entrains air to form bubbles that rise to the water surface and burst to form droplets.[2] Bubble bursting creates both film and jet drops that evaporate to form SSA, with diameter modes near 100 nm and 1−2 μm, respectively.[2,3] SSA particles are largely inorganic salts but also contain organic matter scavenged as bubbles rise through the water column and burst at the surface,[2] which is enriched in organic species with respect to bulk seawater.[4] SSA composition is generally size-dependent, with larger particles containing primarily sodium chloride and smaller particles with an enhanced organic content.[2,5,6] However, recent studies have demonstrated the complexity of the SSA composition,[5,7,8,13,91] for example, observing supermicron particles enriched in organics and the persistence of salts in sub-100 nm particles.[3] The diversity of seawater biology is reflected in the organic compounds observed in the sea surface microlayer (SML) and in SSA particles, including marine colloids or gels,[9−11] aliphatic compounds including fatty acids,[12−15] carbohydrates including monosaccharides and polysaccharides,[8,12,16−18] amino acids,[19−21] proteinaceous material,[19−21] and siliceous material, such as

Received: June 25, 2022
Revised: August 18, 2022
Accepted: August 22, 2022
Published: September 2, 2022

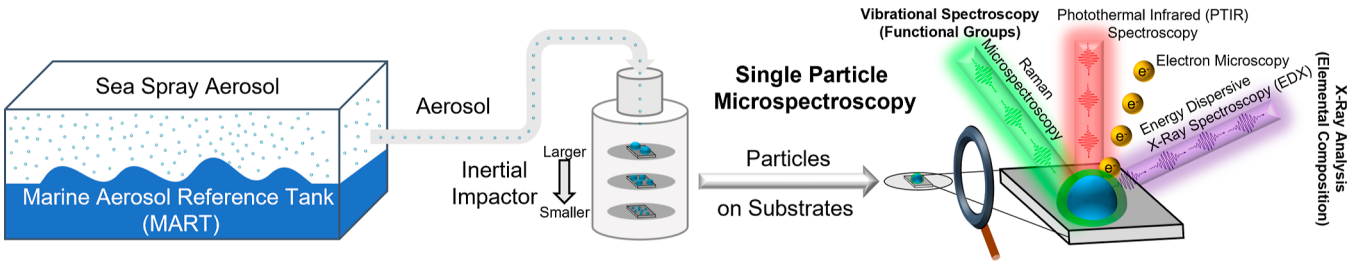

Figure 1. Schematic showing experimental design and analysis by three spectroscopic techniques (computer-controlled scanning-electron microscopy with X-ray energy-dispersive analysis, Raman microspectroscopy, and infrared microspectroscopy). These methods were used to characterize hundreds of individual aerosol particles generated within a MART, simulating SSA production.

diatom fragments.[12,22,23] Ambient SSA studies have identified a complex relationship between seawater biology and the composition of marine dissolved organic matter (DOM) within individual SSA particles.[24,25] There are a limited number of studies on the composition of SSA in the North Atlantic,[6,17,24,26−30] and few of these studies include single-particle measurements.[17,28] Additionally, few studies have examined the effect of salinity changes due to freshwater inputs on aerosol production,[31−34] with the corresponding information about aerosol chemical composition lacking.

The complexity of SSA has led researchers to employ a range of analytical techniques to measure the chemical composition of atmospheric SSA.[2,35,36] Previous microspectroscopy studies have characterized the chemical composition of SSA using scanning or transmission electron microscopy with energy-dispersive X-ray analysis (SEM−EDX/TEM−EDX),[5,32,37−47] Raman microscopy,[12,25,42,45,46,48] IR microspectroscopy,[17,25−27,29,30,49,50] scanning transmission X-ray microscopy with near-edge X-ray absorption fine structure spectroscopy (STXM−NEXAFS),[5,17,37,45,46,51,52] and energy-dispersive electron probe X-ray microanalysis (ED-EPMA).[25] SSA has also been characterized by mass spectrometry techniques, including single-particle mass spectrometry,[12,32,41,44] aerosol mass spectrometry (AMS),[12,29] thermal desorption chemical ionization mass spectrometry (TDCIMS),[27] Fourier transform ion cyclotron resonance mass spectrometry (FT-ICR MS),[53] and liquid chromatography−mass spectrometry (LC/MS).[24] Additional methods employed include nuclear magnetic resonance (NMR) spectroscopy,[6,24,53] synchrotron-induced X-ray fluorescence spectrometry (S-XRF),[43] and single-particle fluorescence spectrometry (GAP-SPFS).[28] Further, bulk concentrations of inorganic ions in SSA particles are often measured using ion chromatography (IC),[27,29,30,49,50] while the concentration of saccharides in bulk SSA has been measured using ion exchange chromatography (IEC) with electrochemical detection.[12]

Despite the plethora of methods that have been applied to SSA, advancing our understanding of the processes involved in SSA generation and its subsequent properties has required combining methods. For example, elemental composition of individual particles is not sufficient to understand the properties of the organic components since it can only provide the amount of carbon, while identifying functional groups using vibrational spectroscopy without elemental information also provides an incomplete picture. Thus, studies that utilize multiple methods are needed, preferably at the single-particle level, given the variations in composition occurring within an aerosol population and even within a single aerosol particle.[54] If an aerosol population is assumed to be chemically homogeneous, which is rare in the actual atmosphere, subsequent effects on atmospheric chemistry and climate are difficult to predict, such as the activation of aerosol particles as cloud condensation nuclei[54] or individual particle reactivity.[55]

To explore the variation in SSA chemical composition, specifically the organic components, Raman microspectroscopy can probe particles below 1 μm, but to date, traditional Beer's law infrared microspectroscopy has been limited to particles $\geq$10 μm. Recently, the development of photothermal infrared spectroscopy (PTIR) has enabled IR spectroscopy of submicron particles when coupled with atomic force microscopy (AFM).[56,57] However, few studies have applied AFM−PTIR to SSA,[58,59] and the need to contact the sample with the tip has made its application to sticky samples challenging. The recent development of optical PTIR (O-PTIR) enables analysis of particles with the same spatial resolution as that of Raman microspectroscopy since the probe laser is the same (532 nm).[60,61] In addition, using an optical probe avoids issues of contact with the surface for AFM−PTIR. PTIR and Raman spectra can also be collected simultaneously from the same particle. This provides information based on both the dipole moment (IR spectroscopy)[17,25−27,29,61] and polarizability (Raman spectroscopy).[42,61] An added benefit of O-PTIR is that it is not influenced by fluorescence, a common challenge for Raman spectroscopy of complex organic species using a 532 nm laser. A third piece of chemical information, elemental composition, is still needed. SEM−EDX can determine the atomic percentage of elements in a particle, with the combination of various elements being distinct for different particle sources, allowing grouping of particles into classes.[32,46,62,63] The combination of Raman spectroscopy, IR spectroscopy, and EDX analysis has the potential to provide unique insights for particles across a key size range for SSA (~500−10,000 nm) in contrast to the use of just one or two techniques.

Herein, we present an analysis of single-particle chemical characterization of SSA for the first time using Raman spectroscopy, O-PTIR spectroscopy, and SEM−EDX. We probe wintertime SSA produced from Gulf of Maine seawater in a series of four laboratory-based experiments using a marine aerosol reference tank (MART). Through this novel combination of analytical measurements, the influence of water temperature, salinity, and dissolved biogenic organic material on the chemical composition of the generated SSA was investigated. The results presented herein have important implications for SSA impacts on climate in cold coastal and estuarial environments, including the Gulf of Maine and marine environments influenced by river outflows or snow and ice melt.

https://doi.org/10.1021/acsmeasuresciau.2c00041
ACS Meas. Sci. Au 2022, 2, 605−619

METHODS

MART and Gulf of Maine Seawater

Four SSA generation experiments (Table S1) were conducted in January 2018 using a MART[64] at the Bigelow Laboratory for Ocean Sciences in East Boothbay, Maine (43°51′35.0″N, 69°34′47.1″W). The experimental design and analysis are summarized in Figure 1. The MART was kept inside the laboratory building during Experiment 1, resulting in a water temperature of 20 ± 3 °C. The MART was then moved outside (where the average ambient temperature fell between −5 and 10 °C), resulting in a water temperature of 11.3 ± 0.3 °C for Experiment 2, 18 ± 2 °C for Experiment 3, and 16 ± 1 °C for Experiment 4 (Table S1). The range of water temperatures measured during the four experiments demonstrates the limits of temperatures that were experimentally feasible given an indoor laboratory setting and temperature control by outdoor ambient air, rather than a systematic evaluation of the effect of temperature on SSA production. Additionally, it should be noted that the room lights were kept on during Experiment 1 and that the MART was exposed to outdoor sunlight during Experiments 2, 3, and 4.

For each experiment, the 210 L MART was filled with 100 L of filtered (0.2 μm Whatman high flow filter cartridge) ambient seawater from the Bigelow seawater intake sampled from the Gulf of Maine. New seawater was collected for each experiment. To probe the influence of dissolved organic material (DOM) on SSA production, the filtrate (0.2 μm Whatman high flow filter cartridge) of a *Haematococcus* microalgal culture, representative of local freshwater inputs, was added to the MART for Experiments 3 and 4, comprising 50% and 66%, respectively, of the total 100 L water volume for each experiment (Table S1). The addition of the microalgal filtrate also changed the salinity for Experiments 3 and 4, as listed in Table S1. Seawater samples were collected from the MART prior to and immediately after each experiment for measurements of dissolved organic carbon (DOC) and total dissolved organic nitrogen (TDN). DOC and TDN were analyzed using a Shimadzu TOC-L system equipped with TNM-L for N detection, located at the University of Miami, following the method described by Dickson et al.,[65] with reference material used for equipment calibration provided by the Hansell Consensus Reference Material (CRM) program.[66] Water temperature was monitored over the course of each experiment using a temperature logger (HOBO Water Temperature Pro v2, Onset) deployed inside the MART tank. The average water temperature for each experiment (Table S1) was calculated for the period over which the temperature and aerosol size distributions were stable.

Aerosol Generation and Particle Collection

The MART employed in this study uses a plunging jet, which produces a bubble plume.[64] Bubbles within this plume rise to the surface of the water and burst, thus producing aerosol particles. The MART bubble plume was optimized with a waterfall cycle of 4 s on and 4 s off with a total 4.5 min on and 0.5 min off cycle. Prior to the SSA experiments, in December 2017, bubble size spectra were measured within the MART for both Gulf of Maine seawater and freshwater (filtered tap water) and optimized to spectra previously determined for wave breaking in seawater[67−71] and freshwater,[72−76] especially in cold regions[67,68] (Figure S1). The Gulf of Maine seawater bubble spectrum was consistent with previous open ocean observations.[67,68,70,77] Under the MART conditions used in this work, freshwater bubble densities were 3 to 6 orders of magnitude lower than seawater bubble densities; in comparison, previous laboratory studies observed freshwater bubble densities 1−3 orders of magnitude lower than seawater bubble densities.[72]

Aerosol particles were sampled from the 110 L headspace in the MART through two diffusion driers to maintain an aerosol flow relative humidity of ∼15%, with a total air flow of 6.3 L min^{-1} from the MART to the aerosol instrumentation. The sampled air flow was balanced by an inflow of 7.0 L min^{-1} of particle-free (1.2 μm pore size HEPA capsule filter, Pall Life Sciences) air to maintain a positive pressure within the MART and eliminate the possibility of sampling room air. The short residence time (∼15 min) within the MART provided sampling of nascent SSA without atmospheric heterogeneous reactions with reactive gases. Before starting the MART waterfall, the tank was purged with particle-free air to ensure aerosol number concentrations of <20 particles/cm^3.

A 10-stage rotating micro-orifice uniform deposit impactor (MOUDI 110R, MSP Corp.) sampled from the MART at 5 L min^{-1}, with an additional 25 L min^{-1} of particle-free air (1.2 μm pore size HEPA capsule filter, Pall Life Sciences) for a total flow rate of 30 L min^{-1}. The MOUDI and aerosol sizing instruments, described below, sampled simultaneously for 6 h. The MOUDI collected SSA particles onto silicon wafers and quartz substrates (Ted Pella, Inc.) for offline single particle analysis, as described below. MOUDI substrates were stored in sealed tubes in the dark at ambient temperature prior to analysis.[78]

Physical Properties: Size and Number Concentration

To measure SSA size distributions and number concentrations, a scanning mobility particle sizer (SMPS, model 3938, TSI Inc.) and an optical particle sizer (OPS, model 3330, TSI Inc.) sampled from the MART at 0.3 and 1.0 L min^{-1}, respectively. For each MART experiment, the SMPS and OPS measured aerosol size distributions (5 min scans each) for particles 14−760 nm (mobility diameter, d_m) and 337−10,000 nm (optical diameter, d_{op}), respectively. Size distributions from the SMPS and OPS were combined following a previously established method[79,80] to determine the total number concentration and particle size modes for each experiment. The OPS distributions were converted to mobility diameter, assuming a shape factor of 1 and a density of 2.0 g/cm^3 (representative of sodium chloride).[81] The SMPS and OPS data were combined, using the SMPS size range from 14 to 737 nm (d_m) and the OPS data from 0.887 to 6.38 μm (d_m) converted from 1.25 to 10.0 μm (d_{op}) (omitting the first six bins that overlapped with the SMPS), for a total distribution from 14 to 6375 nm d_m.

Elemental Composition: Computer-Controlled Scanning Electron Microscopy

Computer-controlled scanning electron microscopy with energy-dispersive X-ray spectroscopy (CCSEM−EDX)[38,82] was conducted for SSA particles collected on silicon from three MOUDI stages (1.0−1.8 μm aerodynamic diameter, d_a, 0.32−0.56 μm d_a, and 0.10−0.18 μm d_a). Analysis was conducted using a FEI Helios Nanolab SEM/FIB instrument equipped with a field emission gun operating at 20 kV accelerating voltage and an Everhart−Thornley secondary electron detector for SEM imaging. X-ray spectra from elements C, N, O, Na, Mg, S, Cl, K, Ca, Ti, Fe, Ni, and Zn were detected using an EDX detector (EDAX, Inc).

CCSEM−EDX analysis of ∼100 SSA particles per substrate provided the size, morphology, and relative abundance of the identified elements in individual SSA particles. EDX has previously been shown to quantitatively reproduce SSA and freshwater (lake spray) aerosol elemental ratios.[5,32,63,72,83,84] K-means clustering of the individual particle EDX spectra for ∼1500 total analyzed particles grouped the particles into 20 clusters based on similarity of elemental composition.[62,85] These clusters were then combined into four main particle types [SSA, SSA + organic carbon (SSA + OC), organic, and Fe- or Ca-containing] based on comparison of the EDX spectra to previous studies of ambient and lab-generated SSA.[45,62,85,86]

Functional Group Analysis: Raman Microspectroscopy

Individual SSA + OC particles on quartz substrates were analyzed by Raman microspectroscopy using a Horiba LabRAM HR Evolution spectrometer coupled with a confocal optical microscope (100× N.A. 0.9 Olympus objective), a Nd:YAG laser (50 mW, 532 nm), and a CCD detector using a 600 groove/mm diffraction grating. Raman spectra were collected over the 500−4000 cm^{-1} range with a spectral resolution of ∼1.8 cm^{-1}. The acquisition time for each Raman spectrum was 30 s, with three accumulations and a 20 s delay. Spectra were compared to prior Raman studies of nascent SSA based on functional group peak assignments.[7,12,87,88] For each experiment, Raman spectra were collected for ∼15−20 individual particles each from two MOUDI

https://doi.org/10.1021/acsmeasuresciau.2c00041
ACS Meas. Sci. Au 2022, 2, 605−619

stages (1.0−1.8 μm d_a and 0.32−0.56 μm d_a) for a total of 150 particles analyzed using Raman microspectroscopy.

Functional Group Analysis: O-PTIR Microspectroscopy

SSA particles collected on quartz substrates were also analyzed by IR microspectroscopy using an mIRage infrared + Raman microscope (Photothermal Spectroscopy Corp.) with a quantum cascade laser (QCL), which allows for the collection of IR spectra in the range 882−1946 cm^{-1} with a spectral resolution of 2 cm^{-1}.[61] The mIRage uses a continuous wave visible laser (532 nm, 200 mW), coaligned with the pulsed, tunable IR laser (QCL) to probe the sample. The mIRage is equipped with a visible objective (4 × 0.13 numerical aperture and 17.3 mm working distance) and a Cassegrain reflective objective (40 × 0.78 numerical aperture and 8.3 mm working distance).

IR spectra were collected using a laser repetition rate of 104.63 kHz, a pulse width of 200 ns, a probe power of 2.5 mW, an IR laser power of 4.8 mW, and a standard detector with 2× gain. A sweep speed of 1000 cm^{-1}/s and an acquisition time of 30 s were used. For each particle, the IR spectra were averaged over 10 accumulations. For each MART experiment, IR spectra were collected for 10−20 individual particles from the same samples that were used for the collection of Raman spectra (the MOUDI stages corresponding with particle diameters of 1.0−1.8 μm d_a and 0.32−0.56 μm d_a).

RESULTS AND DISCUSSION

SSA generation experiments (Table S1) were conducted in January 2018 using Gulf of Maine seawater inside the laboratory at room temperature (20 ± 3 °C, Experiment 1) and outside at a lower water temperature (11.3 ± 0.3 °C, Experiment 2). Experiments 3 and 4 were also conducted outside at lower temperatures (18 ± 2 and 16 ± 1 °C, respectively) with added DOM. Overall, across the four MART experiments, the shape of the aerosol size distribution (Figure 2) was similar, with a smaller mode at ∼120−150 nm and an additional, larger mode at 1.2 μm. The diameter of the smaller mode agrees with the previous studies in which the size distribution mode of ambient

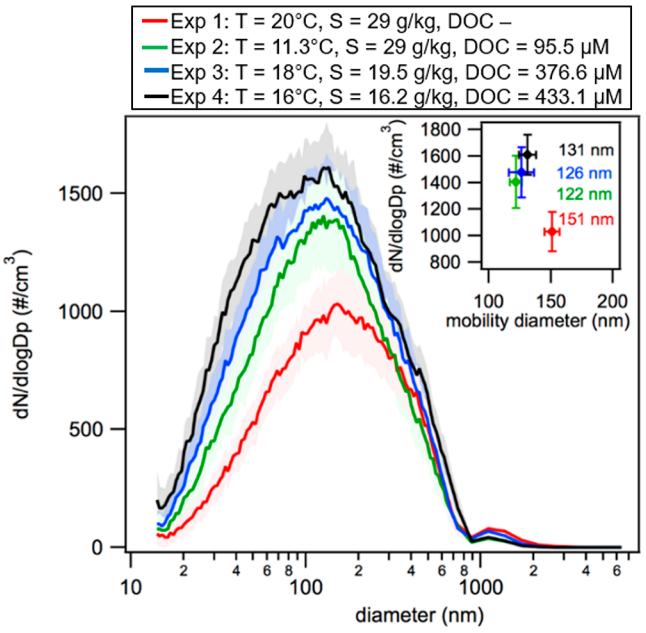

Figure 2. Average aerosol size distributions for each experiment. Shaded regions indicate standard deviations. The inset plot shows the size mode and associated standard deviation for each experiment. The water temperature (T), salinity (S), and dissolved organic carbon (DOC) are listed for each experiment in the legend. Note that DOC was not measured during Experiment 1.

and laboratory-generated SSA particles fell in the range 100−200 nm.[89−91] The prevalence of SSA in the submicron diameter range leads to an analytical challenge in measuring the chemical composition at the individual particle level.

A detailed discussion of the impacts of seawater temperature, DOC, and salinity on generated aerosol concentrations and size distributions is provided in the Supporting Information. Notably, the total number concentration of generated aerosol increased from 1000 ± 100 particles/cm^3 in Experiment 1 to 1300 ± 200 particles/cm^3 in Experiment 2, 1500 ± 200 particles/cm^3 in Experiment 3, and 1700 ± 200 particles/cm^3 in Experiment 4. Two-sample Kolmogorov−Smirnov tests[92,93] (95% significance level) were carried out for each pair of experiments to determine if the aerosol size distributions were significantly different. The p-value for this test fell below 0.05 for each pair aside from Experiment 2 and Experiment 3 (p = 0.22), indicating that these two aerosol size distributions were not statistically different at the 95% significance level. The largest changes in the aerosol particle size distribution (both mode diameter and total number concentrations) occurred between Experiments 1 and 2, when the water temperature decreased from 20 ± 3 to 11.3 ± 0.3 °C, consistent with previous temperature-dependent SSA generation studies.[94−96] A decrease in salinity occurred alongside an increase in DOC between Experiments 2 and 3, though it is difficult to compare the effects of salinity and DOC on the aerosol size distribution between these two experiments due to a simultaneous change in temperature. However, the salinity (and likely also DOC) was identical in Experiments 1 and 2, while the water temperature was similar in Experiments 1 and 3. Therefore, the statistically significant difference in the aerosol size distributions measured in Experiments 1 and 3 may be attributed to an increase in DOC and/or a decrease in salinity. This same trend was observed between Experiments 3 and 4, when an additional aliquot of the filtrate further increased the DOC concentration and decreased the salinity of the seawater, resulting in another statistically significant increase in the aerosol size distribution between these two experiments. It should be noted that the mode diameter changed very little with DOC concentration and salinity between Experiments 2, 3, and 4; this result is in agreement with a previous study in which the mode diameter of SSA generated from seawater (salinity ≈ 27 g/kg) was nearly identical to that of SSA generated from water collected from a coastal sea site (salinity = 19.5−25.3 g/kg).[31] In summary, a decrease in the temperature of the seawater from 20 ± 3 to 11.3 ± 0.3 °C produced a statistically significant increase in the concentration of generated aerosol particles, while increases in DOC concentration, paired with decreases in salinity, led to smaller, but statistically significant, increases in generated aerosol concentration when the temperature was maintained within the range 16−20 °C.

Elemental Analysis of SSA Composition Using CCSEM−EDX

The elemental composition of 0.12−7.05 μm individual particles generated in each MART experiment was measured using CCSEM−EDX. From the resulting 2499 EDX spectra, four main particle types were identified, including SSA (primarily salts), SSA internally mixed with organic carbon (SSA + OC), organic carbon particles (without salts), and Fe- or Ca-rich particles (Figure 3). These particle types are consistent with results from previous studies on aerosol particles generated from MARTs using natural seawater.[41] SSA particles were characterized as containing primarily Na and Cl, at elemental

https://doi.org/10.1021/acsmeasuresciau.2c00041
ACS Meas. Sci. Au 2022, 2, 605−619

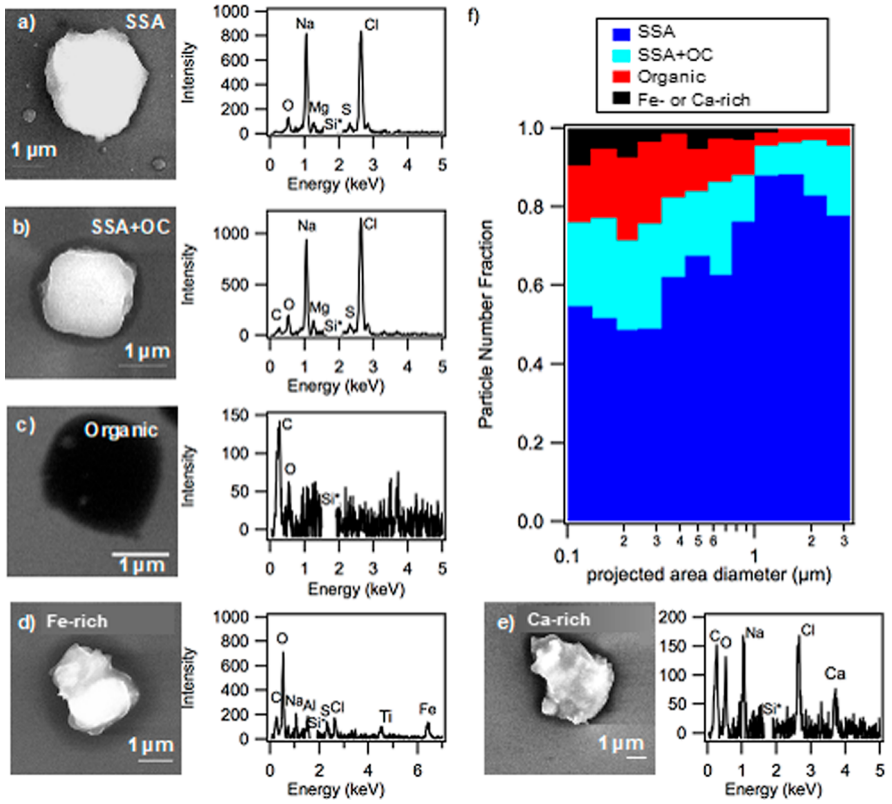

Figure 3. Representative SEM images and EDX spectra of observed particle types including (a) sea spray aerosol (SSA), (b) sea spray aerosol with organics (SSA + OC), (c) organic aerosol, (d) Fe-dominant particles, and (e) Ca-dominant particles. *Spectra were background-subtracted to remove the signal from the silicon substrate, and the silicon peak was removed for clarity. (f) Size-resolved CCSEM−EDX number fraction distributions of observed particle types.

ratios of 0.94−1.16, similar to the seawater Cl/Na ratio of 1.16.[2,81,97] SSA + OC were SSA particles enriched in C and O, with at least 2% C in the EDX spectra.[5,25] For the total observed sea salt-containing particles (SSA and SSA + OC), Cl/Na elemental ratios were determined for individual particles from their EDX spectra.[97] Overall, individual supermicron SSA (SSA and SSA + OC, 1.0−1.8 μm d_a) Cl/Na ratios were similar to the seawater ratio (1.16 for Experiments 1−3 and 1.15 for Experiment 4; Figure 4a), consistent with fresh SSA production.[2,81] The method used for calculating the seawater Cl/Na ratio is discussed in the Supporting Information. The SSA Cl/Na ratios for stage 9 (0.10−0.18 μm d_a) were slightly lower relative to seawater, particularly for Experiment 3 (average Cl/Na ratio 0.94) and Experiment 4 (average Cl/Na ratio 0.95) with added DOM. Submicron SSA Cl depletion has been previously observed and related to increased biological content.[97,98]

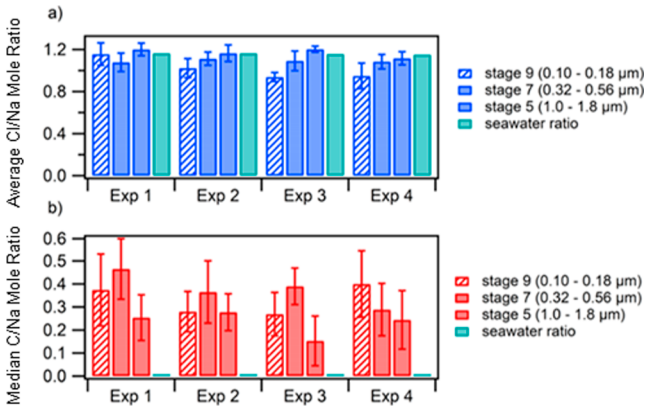

Figure 4. (a) Average individual SSA and SSA + OC particle Cl/Na and (b) average C/Na mole ratios measured using EDX for each MART experiment and MOUDI size range, compared to initial MART values measured for the water. The method used for calculating the seawater Cl/Na and C/Na ratio is discussed in the Supporting Information.

Organic particles were primarily composed of C and O, with 23% of these particles, by number, also containing S and 5%, by number, containing N. EDX can be less sensitive to N such that the number fraction of particles containing N represents a lower limit.[99] Organic particles were most prevalent at sizes smaller than 500 nm (d_a). Previous studies have shown that organic particles are smaller than sea salt-containing aerosols, with the majority of organic particles produced from sea spray falling within the submicron range.[5,41,44,45] The circular morphology of these organic particles is indicative of non-viscous particles (Figure 3), consistent with the transfer of marine organics from the SML to the particle phase via bubble bursting.[3,5,52] Fe- or Ca-rich particles comprised less than 5−10% of the particle number across the observed size range but were present in all experiments (Figure S2). These particles contained Ca or Fe as the primary cation, with smaller amounts of Na and Cl, in addition to organics.[100,101] In comparison, SSA and SSA + OC particles only contained small amounts (<5 relative atomic percent) of Ca and no detectable Fe. The presence and composition of these Ca-rich particles (Figure S3) are consistent with previous observations of calcium enrichment in submicron SSA.[98,100,102] Increases in iron-containing particles and those

https://doi.org/10.1021/acsmeasuresciau.2c00041
ACS Meas. Sci. Au 2022, 2, 605−619

containing divalent cations (Mg and Ca) mixed with organic content have also been observed after nutrient addition to mesocosm experiments.[8,100]

The relative number fractions of all four main particle types (SSA, SSA + OC, organic, and Fe- or Ca-enriched) were similar across the four MART experiments (Figure S2). At supermicron diameters (1.0−4.0 μm), SSA particles accounted for most of the observed particles, ∼80% by number, with number fractions of ∼60% for submicron diameters (0.1−1.0 μm) (Figures 3 and S2). At submicron diameters (0.1−1.0 μm), increased number fractions of SSA + OC and organic particles were observed, comprising ∼15−32 and ∼6−20% of particles, by number, respectively, as compared to ∼8−18 and 1−5% at supermicron diameters (Figure 3). This size dependence of SSA organic content has been observed in previous studies, in which SSA, SSA + OC, and organic particle types were observed.[5,41,90,96,103,104] The presence of SSA + OC and organic particles indicates influence of seawater biology through the transfer of SML and/or seawater column organic content to the particle phase.[2,12,25,41,58] While this size dependence in organic content was observed, similar number fractions were observed for experiments with natural seawater (Experiments 1 and 2) and those with added microalgal filtrate (Experiments 3 and 4), suggesting that the amount of DOM present did not dramatically affect the distribution of the observed particle types within the population of aerosol particles generated during the MART experiments. However, the observed number fractions of SSA and SSA + OC particle types do not reflect the mass of organic material present in the individual SSA + OC particles; therefore, individual SSA particle carbon content was examined next.

Organic enrichment in salt-containing (SSA and SSA + OC) particles was observed for all experiments and particle size ranges (Figure 4), with individual particle C/Na ratios (median ratios of 0.16−0.47) greatly enriched to above the measured seawater ratio (0.0002−0.003). The method used for calculating the seawater C/Na ratio is discussed in the Supporting Information. While the enrichment of organic material in the particle phase is consistent with previous mesocosm studies,[90,98,100,105] SSA particles are often collected on TEM grids[38,42,44,97,106,107] or polytetrafluoroethylene (PTFE) filters,[108] and the carbon content of particles cannot be accurately quantified on these carbon-rich substrates. The individual particle C/Na ratios were of similar magnitude for all experiments and size ranges (Figure 4b). These results show no significant size dependence in SSA composition, with submicron median C/Na mole ratios of 0.27−0.40 for 0.10−0.18 μm particles and median C/Na mole ratios of 0.29−0.47 for 0.32−0.56 μm particles, compared to supermicron median C/Na mole ratios of 0.15−0.28 for 1.0−1.8 μm particles. Notably, no significant differences were observed in the C/Na ratios between experiments with natural seawater (Experiments 1 and 2) and experiments with the added algal culture filtrate (Experiments 3 and 4), suggesting that the increased DOC did not have a significant influence on SSA organic content at smaller particle diameters.

Characterization of Organic Compounds in SSA + OC Particles Using Raman Microspectroscopy

Raman microspectroscopy was used to characterize the functional groups present within the organic components of the individual SSA + OC particles. Of the 229 particles analyzed, 7% fluoresced, masking the Raman signal. Fluorescence is often indicative of conjugation within biological molecules present in particles.[20,63] An additional 36% of particles were characterized by Raman spectra which contained weak Raman peaks corresponding with common organic modes that could not be confidently distinguished (trace organics), leaving 57% of analyzed SSA + OC particles, by number, with characterizable Raman signals. These Raman spectra were averaged, as shown in Figure 5a for the 1.0−1.8 μm d_a particle diameter range and Figure 5b for the 0.32−0.56 μm d_a particle diameter range; the full set of Raman spectra are shown in Figure S4.

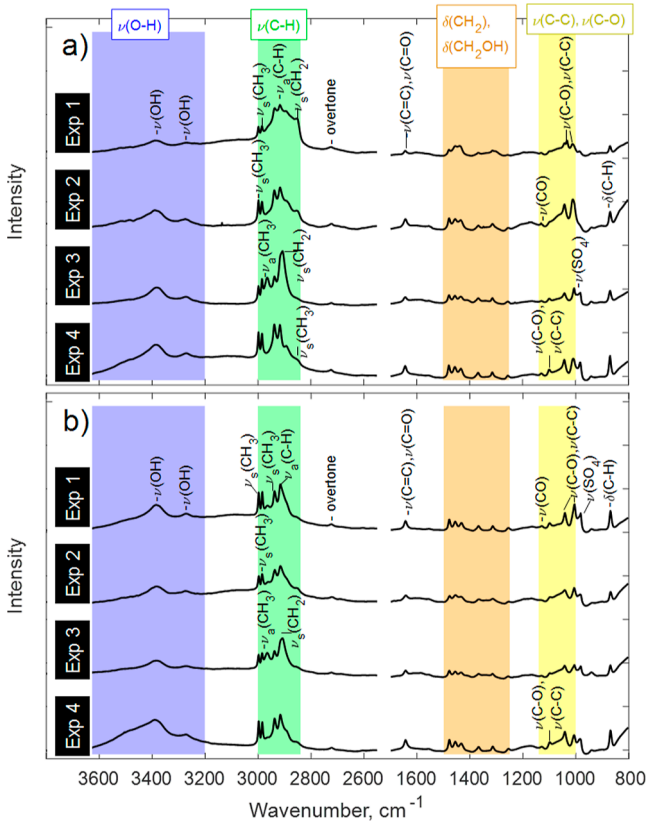

Figure 5. Average individual particle Raman spectra for particles with aerodynamic diameters of (a) 1.0−1.8 μm d_a and (b) 0.32−0.56 μm d_a.

The two major organic composition types in the SSA particles were saccharides and fatty acids. Representative Raman spectra of particles with organic coatings composed primarily of saccharides and fatty acids are shown in Figure 6. Characteristic saccharide peaks include δ(CH) (870 cm^{-1})[12] and ν(C−O) and ν(C−C) (1006, 1040, 1100, and 1129 cm^{-1}).[12,109−113] Saccharide modes corresponding with $\delta(CH_2)$[110,112,114,115] and/or $\delta(CH_2OH)$[12,109,111,113] include 1256, 1314, and 1366 cm^{-1} and a triplet at 1432, 1455, and 1479 cm^{-1}. A common mode at 1640 cm^{-1} is tentatively assigned to (C═O).[12,109] CH, CH_2, and CH_3 stretching characteristics of saccharides included ν(C−H)[12,111,115,116] at 2915 cm^{-1}, $\nu_a(CH_2)$[109] or $\nu_s(CH_2)$[115,116] at 2935 cm^{-1}, $\nu_s(CH_3)$[12] or $\nu_a(CH_2)$[115,116] at 2985 cm^{-1}, and $\nu_s(CH_3)$[12] or $\nu_a(CH_2)$[115,116] at 2995 cm^{-1}. A ν(O−H)[12,87] mode at 3275−3408 cm^{-1} is also observed in many individual particle Raman spectra. The frequency of saccharide modes in SSA + OC particles varied little across experiments or particle size ranges (Figure 7). Saccharides have previously been identified in the seawater SML and in the particle phase.[8,16,21,25,117−119] The prevalence of these modes

https://doi.org/10.1021/acsmeasuresciau.2c00041
ACS Meas. Sci. Au 2022, 2, 605−619

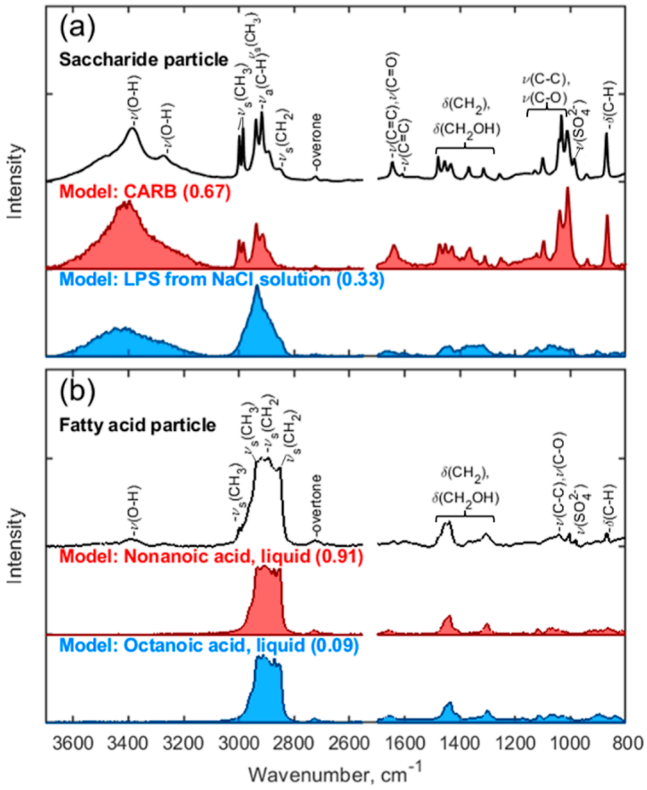

Figure 6. Representative particles identified as (a) saccharide and (b) fatty acid are shown, as well as the closest (red) and second closest (blue) matches from the library of Raman spectra from Cochran et al. 2017. The particles in (a,b) were generated during Experiment 1 and have aerodynamic particle diameters in the range 1.0−1.8 μm. The fractions in parentheses indicate relative contribution of each library spectrum to the best linear combination for the experimental spectrum.

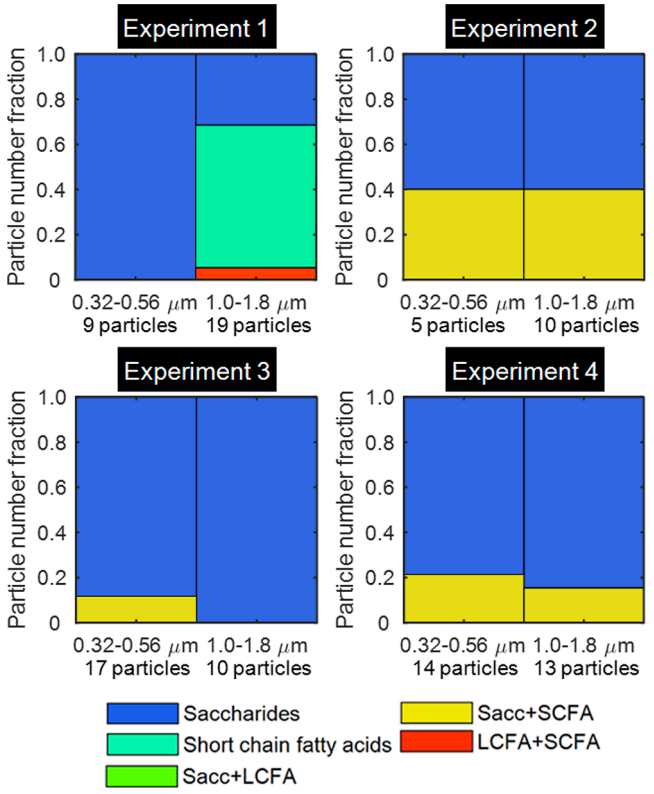

Figure 7. Number fractions of individual SSA + OC particles collected during each experiment that were classified as saccharides (Sacc), long-chain fatty acids (LCFAs), short-chain fatty acids (SCFAs), amino acids, or a combination of two of these categories, based on their Raman spectra. The results of this comparison are shown for each experiment and particle size range (d_a). The number of particles analyzed for each sample are shown as well.

suggests that saccharides are abundant in Gulf of Maine seawater and may preferentially transfer into the aerosol phase.

Modes characteristic of fatty acids included $\delta(CH_2)$ and $\delta(CH_3)$ (1444 cm^{-1}),[12,87,110,120] a CH rock overtone (2724 cm^{-1}),[12,109,120] and CH_2 and CH_3 stretching modes (2853, 2880, 2894, 2904, and 2965 cm^{-1}).[12,109,120,121] Of these modes, 1444 and 2853 cm^{-1} were observed in a greater number fraction of the SSA + OC individual particle Raman spectra collected from supermicron (1.0−1.8 μm d_a) particles generated during Experiment 1 (39 and 45%) than from other experiments, regardless of the particle diameter (0−6 and 0−22%, respectively). Experiment 3 was also marked by unique fatty acid modes; the Raman spectra of 64%, by number, of the supermicron SSA + OC particles and 50% of the submicron SSA + OC particles collected during Experiment 3 contained the stretching mode at 2904 cm^{-1} (compared to 0−18% of the other samples), while 100%, by number, of the supermicron SSA + OC particles and 89% of the submicron particles collected during Experiment 3 contained the stretching mode at 2965 cm^{-1} (compared to 0−73% of the other samples). Fatty acids have previously been observed in SSA,[14,122−124] though few studies have identified fatty acids in individual SSA particles.[12,25]

Sulfate symmetric stretching modes [$\nu_s(SO_4^{2-})$ from 975 to 984 cm^{-1}][109,125−127] were identified in 0−71%, by number, of the Raman spectra of supermicron (1.0−1.8 μm d_a) SSA + OC particles and 25−87% of the Raman spectra of submicron (0.32−0.56 μm d_a) particles. In addition, some of the modes from 1004 to 1015 could be from calcium sulfate or magnesium sulfate,[87] which often co-locate during drying on the substrates.[5] Sulfate has been identified as a component in nascent SSA in some studies,[87,128] though it is more prevalent in aged SSA following chlorine depletion and sulfur enrichment.[129−131] Notable absences from the Raman spectra include modes characteristic of phosphate (940−960 cm^{-1}),[109,132,133] bisulfate (1040−1053 cm^{-1}),[109,126] nitrate (1040−1068 cm^{-1}),[83,109] carbonate (1065−1094 cm^{-1}),[109,134] ammonium (1410−1417 cm^{-1}, though this ammonium mode is only weakly Raman active),[109,135] and C═O esters (1736 cm^{-1}).[110] A list of Raman mode assignments is given in Table S2.

It should be noted that SSA + OC particles from Experiments 3 and 4, with the added microalgal culture filtrate, did not show distinct evidence of the added *Haematococcus*-derived DOM in the Raman spectra. The carotenoid astaxanthin is a major component of *Haematococcus* and is expected to have strong Raman modes at 1157 cm^{-1} for ν(C−C) and 1520 cm^{-1} for ν(C═C), which were not observed in the particle spectra.[136,137] Degradation of the astaxanthin molecule during filtration or through the water cycling process in the MART may result in similar free saccharide modes to those observed.

The individual SSA + OC particle Raman spectra were also quantitatively compared with a library of 64 Raman spectra of organic compounds including saccharides, long-chain fatty acids (LCFAs), short-chain fatty acids (SCFAs), and amino acids, using χ^2 analysis in order to determine the two best matches for each particle.[12] The linear combination of these library spectra that best fit the experimental Raman spectrum was then

https://doi.org/10.1021/acsmeasuresciau.2c00041
ACS Meas. Sci. Au 2022, 2, 605−619

determined.[12] Two individual particle examples of this analysis are shown in Figure 6; the models shown here are from Cochran et al. The number fractions of SSA + OC particles analyzed that included saccharides, LCFAs, SCFAs, and/or amino acids in their top two Raman library matches are shown in Figure S5. None of the analyzed particles matched with any of the amino acids in the library.

The individual SSA + OC particle spectra were placed into categories (saccharides, LCFAs, SCFAs, saccharides + LCFAs, saccharides + SCFAs, saccharides + amino acids, LCFAs + SCFAs, and SCFAs + amino acids) based on their top library matches. The results of this analysis are shown in Figure 7. The most common categories observed were saccharides (similar to the particle shown in Figure 6a) and saccharides combined with SCFAs (Figure 7). One supermicron (1.0−1.8 μm d_a) particle collected during Experiment 1 matched with an LCFA as well. Although the overall composition of the organic coatings on the SSA particles generally varied little between experiments, a larger fraction of supermicron particles matched with the fatty acid Raman spectra in Experiment 1 than other samples, consistent with the prevalence of the modes 1444 and 2853 cm^{-1} observed in these particle spectra.

The most common Raman library spectra that identified as one of the top two matches in the χ^2 analysis were five saccharides: carbohydrates (30 particles, abbreviated as CARB in Figure 6), lipopolysaccharides from NaCl solution (29 particles), lipopolysaccharides from water (21 particles), L-arabitol (21 particles), and sucrose (16 particles). The library spectrum collected from aged lipopolysaccharides is also a close visual match to many of the spectra collected during this study, similar to the spectrum shown in Figure 6a. A few SCFAs, including octanoic acid (10 particles), nonanoic acid (10 particles), and hydroxyhexanoic acid (7 particles) were common matches as well.

Characterization of Organic Coatings on SSA + OC Particles Using Infrared Microspectroscopy

The IR spectra from individual SSA + OC particles exhibited common modes corresponding with ν(C−O) and ν(C−O−C) (1128, 1173, and 1257 cm^{-1}).[109,116,138−142] Modes corresponding with various C−H vibrations were also common, including $\delta(CH_2)$ and $\delta(CH_3)$ (1313 cm^{-1}),[143,144] CH_2 wag (1368 cm^{-1}),[116] $\delta(CH_3)$ (1378 cm^{-1}),[120,121,140,142,145,146] and $\delta(CH_2)$ (1430 and 1478 cm^{-1}),[116,120,121,138,147−149] In agreement with the Raman analysis, modes corresponding with ν(C═O) (1650 cm^{-1})[140,150,151] were observed in most of the IR spectra. A few IR spectra contained modes characteristic of the antisymmetric stretch of the sulfate anion [$\nu_{as}(SO_4^{2-})$, 1094−1111].[141,152−156] The averaged IR spectra from each experiment and MOUDI stage are shown in Figure 8, and the full set of IR spectra are shown in Figure S6.

Similar to the Raman spectra, the IR spectra notably did not include modes characteristic of phosphate (1000−1080 cm^{-1}),[109,156,157] bisulfate (1029−1050 and 1133−1215 cm^{-1}),[150,156,158−160] nitrate (1318−1383 cm^{-1}),[150,152,156,161] carbonate (1429−1460 cm^{-1}),[109,156,162] ammonium (1410−1435 cm^{-1}),[142,150,152,156] or C═O esters (1740−1746 cm^{-1}).[140,146] The amide II peak (1517−1150 cm^{-1})[140,163,164] was also absent, which provides additional evidence that amino acids were not a predominant component of the SSA + OC particles generated during the four experiments. A list of IR mode assignments is given in Table S3.

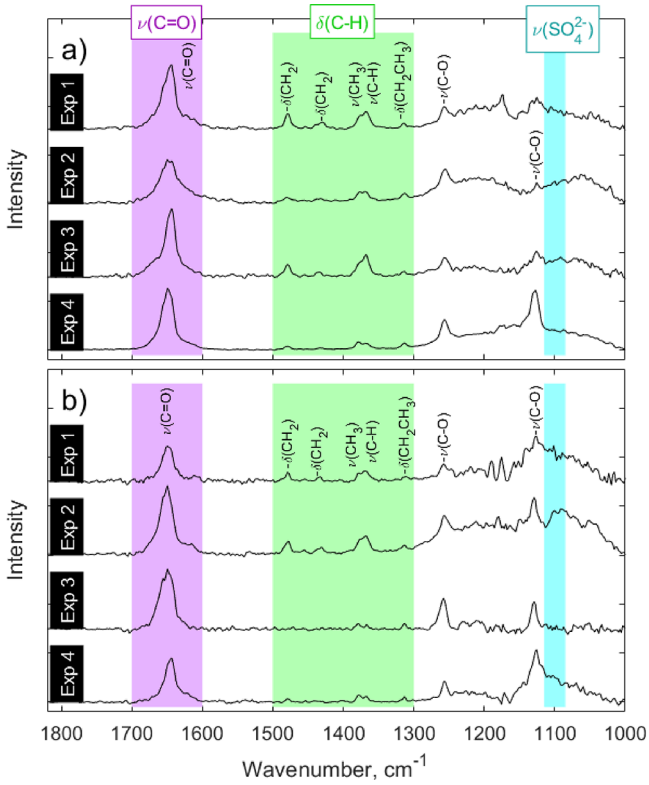

Figure 8. Average individual particle IR spectra for particles with aerodynamic diameters of (a) 1.0−1.8 μm d_a and (b) 0.32−0.56 μm d_a.

The Raman and IR spectra show that organic species, primarily consisting of saccharides with a smaller contribution from fatty acids, were transferred from the seawater in the MART to the aerosol phase as coating on sea salt particles. A greater fraction of fatty acids was observed in the supermicron SSA + OC particles generated during Experiment 1, but otherwise, the composition of the organic coatings on the SSA + OC particles was consistent across the four MART experiments regardless of variations in water temperature, salinity, and DOC concentration.

CONCLUSIONS

The multi-method measurement of SSA composition on the scale of individual particles is necessary for the accurate representation of the chemical state of this highly abundant aerosol source globally. Single-particle measurements of elemental composition and functional groups that elucidate the mixing state and contributions from marine organic compound groups (e.g., saccharides and fatty acids), as shown herein, are critical. Changes in SSA size distributions, number concentrations, and chemical composition due to seawater temperature, salinity, and DOC are necessary in order to predict the impacts of SSA on clouds and climate. These impacts are especially important for constraining changes in rapidly changing cold marine environments, areas of changing salinity, and regions of dynamic or enriched biological activity,[165] including estuaries, river outflows, and areas of snow or ice melt. To this end, four SSA generation experiments were conducted using a MART with wintertime Gulf of Maine seawater and added DOM from a *Haematococcus* microalgal culture filtrate. The influences of seawater temperature, biology, and salinity on aerosol production and individual particle composition were

https://doi.org/10.1021/acsmeasuresciau.2c00041
ACS Meas. Sci. Au 2022, 2, 605−619

investigated. The chemical composition of the individual particles was probed using a multi-modal approach employing CCSEM−EDX, Raman microspectroscopy, and O-PTIR microspectroscopy.

Statistically significant increases in aerosol particle concentrations were observed with decreases in temperature (while salinity and DOC concentration were held constant) and with a simultaneous increase in DOC concentration and decrease in salinity (while water temperature was maintained in the range 16−20 °C). For all experiments, the dominant particle type determined using CCSEM−EDX was inorganic SSA, accounting for 60% of submicron and 80% of supermicron particles, by number. SSA + OC (organic-coated sea salts) and organic particles were observed at greater number fractions in the submicron size range (15−32 and 6−20% of submicron particles, respectively) than in the supermicron size range (8−18 and 1−5%, respectively). The small number fractions of Ca and Fe metal-containing particles observed (5−10%, by number) were most likely related to the seawater biological activity, as observed previously during algal blooms.[8,102,166] The observed individual SSA particle composition was influenced by seawater organics, with carbon enrichments (C/Na ratios of 0.005−0.36) relative to seawater (C/Na ratios of 0.0002−0.003) observed across all particle sizes.[98] Negligible variations in SSA Cl/Na and C/Na ratios were observed between the four experiments, indicating that the ranges in water temperature, DOC concentration, and salinity explored within this study do not appreciably modify the elemental composition of SSA.

Raman and O-PTIR spectra of individual SSA + OC particles showed that the organic component of these particles was dominated by saccharides, with some contribution from fatty acids. Little variation in the composition of this organic component was observed across the four experiments. The multi-modal approach to functional group analysis used in this study strengthens the assignment of organic particle classes to the organic-containing SSA particles.

Determining the influence of temperature, salinity, and marine biology on SSA size distributions and chemical composition is crucial for predicting SSA production and climate impacts in dynamic marine environments, including temperate and polar regions of varying salinity and microbial activity.

■ ASSOCIATED CONTENT

Supporting Information

The Supporting Information is available free of charge at https://pubs.acs.org/doi/10.1021/acsmeasuresciau.2c00041.

Dependence of SSA production on temperature, DOC, and salinity; summary of MART experiments and measured seawater parameters; MART bubble spectra plot; size-resolved CCSEM−EDX number fractions of observed particle types for each experiment; digital color histograms showing the elemental composition of Fe- and Ca-containing particles; Raman spectra collected for SSA + OC particles; number fractions of SSA + OC particles identified as saccharides, LCFAs, SCFAs, and amino acids; Raman spectra of the eight most common model spectral matches for SSA + OC particles; IR spectra collected for SSA + OC particles; peak assignments for vibrational modes observed in individual SSA + OC particle Raman spectra; and peak assignments for vibrational modes observed in individual SSA + OC particle IR spectra (PDF)

■ AUTHOR INFORMATION

Corresponding Authors

Andrew P. Ault − *Department of Chemistry, University of Michigan, Ann Arbor, Michigan 48109, United States;* orcid.org/0000-0002-7313-8559; Email: aulta@umich.edu

Kerri A. Pratt − *Department of Chemistry, University of Michigan, Ann Arbor, Michigan 48109, United States; Department of Earth and Environmental Sciences, University of Michigan, Ann Arbor, Michigan 48109, United States;* orcid.org/0000-0003-4707-2290; Email: prattka@umich.edu

Authors

Jessica A. Mirrielees − *Department of Chemistry, University of Michigan, Ann Arbor, Michigan 48109, United States*

Rachel M. Kirpes − *Department of Chemistry, University of Michigan, Ann Arbor, Michigan 48109, United States;* orcid.org/0000-0002-2998-0108

Savannah M. Haas − *Department of Chemistry, University of Michigan, Ann Arbor, Michigan 48109, United States; Department of Chemistry, Villanova University, Villanova, Pennsylvania 19085, United States*

Carlton D. Rauschenberg − *Bigelow Laboratory for Ocean Sciences, East Boothbay, Maine 04544, United States*

Patricia A. Matrai − *Bigelow Laboratory for Ocean Sciences, East Boothbay, Maine 04544, United States*

Allison Remenapp − *Department of Chemistry, Villanova University, Villanova, Pennsylvania 19085, United States*

Vanessa L. Boschi − *Department of Chemistry, Villanova University, Villanova, Pennsylvania 19085, United States;* orcid.org/0000-0003-4072-1788

Amanda M. Grannas − *Department of Chemistry, Villanova University, Villanova, Pennsylvania 19085, United States;* orcid.org/0000-0003-4719-348X

Complete contact information is available at: https://pubs.acs.org/10.1021/acsmeasuresciau.2c00041

Author Contributions

J.A.M. and R.M.K. contributed equally to this work. J.A.M. and R.M.K. wrote the manuscript. J.A.M., R.M.K., K.A.P., and A.P.A. led data interpretation and synthesis. K.A.P., P.A.M., A.P.A., and A.M.G. designed the project. R.M.K., A.P.A., and C.D.R. designed the experimental setup. R.M.K., C.D.R., and A.R. ran the experiments, with assistance from P.A.M., V.B., and A.M.G. R.M.K. conducted the CCSEM−EDX analysis. J.A.M., R.M.K., and S.M.H. collected the Raman data. J.A.M. collected the PTIR data. All authors have given approval to the final version of the manuscript. CRediT: **Jessica A Mirrielees** formal analysis (equal), investigation (equal), methodology (equal), visualization (equal), writing-original draft (lead), writing-review & editing (equal); **Rachel Martha Kirpes** data curation (equal), formal analysis (equal), investigation (equal), methodology (equal), writing-original draft (lead), writing-review & editing (equal); **Savannah M. Haas** formal analysis (supporting), methodology (supporting), writing-review & editing (supporting); **Carlton D Rauschenberg** conceptualization (supporting), formal analysis (supporting), investigation (supporting), writing-review & editing (supporting); **Patricia A Matrai**

https://doi.org/10.1021/acsmeasuresciau.2c00041
ACS Meas. Sci. Au 2022, 2, 605−619

conceptualization (equal), project administration (equal), writing-review & editing (equal); **Allison Remenapp** formal analysis (supporting), writing-review & editing (supporting); **Vanessa L Boschi** formal analysis (supporting), writing-review & editing (supporting); **Amanda M. Grannas** conceptualization (equal), project administration (equal), writing-original draft (supporting), writing-review & editing (supporting); **Kerri A. Pratt** conceptualization (equal), project administration (equal), writing-original draft (equal), writing-review & editing (equal); **Andrew P Ault** conceptualization (equal), methodology (equal), project administration (equal), writing-original draft (supporting), writing-review & editing (equal).

Notes

The authors declare no competing financial interest.

■ ACKNOWLEDGMENTS

This work was funded by the National Science Foundation (OPP-1724585 to K.A.P. and A.P.A., 1724651 to P.A.M., and 1724642 to A.M.G.). SH was supported by the University of Michigan REU Program in the Chemical Sciences (CHE-1460990). R.M.K. was supported in part by a University of Michigan Department of Chemistry fellowship. For CCSEM–EDX analysis, we acknowledge the Michigan Center for Materials Characterization for use of the instruments and staff assistance. The scanning probe microscopy facility in the Department of Chemistry is acknowledged for O-PTIR analysis.

■ REFERENCES

(1) de Leeuw, G.; Andreas, E. L.; Anguelova, M. D.; Fairall, C. W.; Lewis, E. R.; O'Dowd, C.; Schulz, M.; Schwartz, S. E. Production Flux of Sea Spray Aerosol. *Rev. Geophys.* **2011**, *49*, RG2001.

(2) Quinn, P. K.; Collins, D. B.; Grassian, V. H.; Prather, K. A.; Bates, T. S. Chemistry and Related Properties of Freshly Emitted Sea Spray Aerosol. *Chem. Rev.* **2015**, *115*, 4383−4399.

(3) Wang, X.; Deane, G. B.; Moore, K. A.; Ryder, O. S.; Stokes, M. D.; Beall, C. M.; Collins, D. B.; Santander, M. V.; Burrows, S. M.; Sultana, C. M.; Prather, K. A. The Role of Jet and Film Drops in Controlling the Mixing State of Submicron Sea Spray Aerosol Particles. *Proc. Natl. Acad. Sci.* **2017**, *114*, 6978−6983.

(4) Matrai, P. A.; Tranvik, L.; Leck, C.; Knulst, J. C. Are High Arctic surface Microlayers a Potential Source of Aerosol Organic Precursors? *Mar. Chem.* **2008**, *108*, 109−122.

(5) Ault, A. P.; Moffet, R. C.; Baltrusaitis, J.; Collins, D. B.; Ruppel, M. J.; Cuadra-Rodriguez, L. A.; Zhao, D. F.; Guasco, T. L.; Ebben, C. J.; Geiger, F. M.; Bertram, T. H.; Prather, K. A.; Grassian, V. H. Size-Dependent Changes in Sea Spray Aerosol Composition and Properties with Different Seawater Conditions. *Environ. Sci. Technol.* **2013**, *47*, 5603−5612.

(6) Facchini, M. C.; Rinaldi, M.; Decesari, S.; Carbone, C.; Finessi, E.; Mircea, M.; Fuzzi, S.; Ceburnis, D.; Flanagan, R.; Nilsson, E. D.; de Leeuw, G.; Martino, M.; Woeltjen, J.; O'Dowd, C. D. Primary Submicron Marine Aerosol Dominated by Insoluble Organic Colloids and Aggregates. *Geophys. Res. Lett.* **2008**, *35*, L17814.

(7) Ebben, C. J.; Ault, A. P.; Ruppel, M. J.; Ryder, O. S.; Bertram, T. H.; Grassian, V. H.; Prather, K. A.; Geiger, F. M. Size-Resolved Sea Spray Aerosol Particles Studied by Vibrational Sum Frequency Generation. *J. Phys. Chem. A* **2013**, *117*, 6589−6601.

(8) Jayarathne, T.; Sultana, C. M.; Lee, C.; Malfatti, F.; Cox, J. L.; Pendergraft, M. A.; Moore, K. A.; Azam, F.; Tivanski, A. V.; Cappa, C. D.; Bertram, T. H.; Grassian, V. H.; Prather, K. A.; Stone, E. A. Enrichment of Saccharides and Divalent Cations in Sea Spray Aerosol During Two Phytoplankton Blooms. *Environ. Sci. Technol.* **2016**, *50*, 11511−11520.

(9) Decho, A. W.; Gutierrez, T. Microbial Extracellular Polymeric Substances (EPSs) in Ocean Systems. *Front. Microbiol.* **2017**, *8*, 922.

(10) Chin, W.-C.; Orellana, M. V.; Verdugo, P. Spontaneous Assembly of Marine Dissolved Organic Matter into Polymer Gels. *Nature* **1998**, *391*, 568−572.

(11) Bigg, E. K.; Leck, C. The Composition of Fragments of Bubbles Bursting at the Ocean Surface. *J. Geophys. Res.: Atmos.* **2008**, *113*, D11209.

(12) Cochran, R.; Laskina, O.; Trueblood, J.; Estillore, A.; Morris, H.; Jayarathne, T.; Sultana, C.; Lee, C.; Lin, P.; Laskin, J.; Laskin, A.; Dowling, J.; Qin, Z.; Cappa, C.; Bertram, T.; Tivanski, A.; Stone, E.; Prather, K.; Grassian, V. Molecular Diversity of Sea Spray Aerosol Particles: Impact of Ocean Biology on Particle Composition and Hygroscopicity. *Chem* **2017**, *2*, 655−667.

(13) Kawamura, K.; Bikkina, S. A Review of Dicarboxylic Acids and Related Compounds in Atmospheric Aerosols: Molecular Distributions, Sources and Transformation. *Atmos. Res.* **2016**, *170*, 140−160.

(14) Bikkina, P.; Kawamura, K.; Bikkina, S.; Kunwar, B.; Tanaka, K.; Suzuki, K. Hydroxy Fatty Acids in Remote Marine Aerosols over the Pacific Ocean: Impact of Biological Activity and Wind Speed. *ACS Earth Space Chem.* **2019**, *3*, 366−379.

(15) Kanakidou, M.; Seinfeld, J. H.; Pandis, S. N.; Barnes, I.; Dentener, F. J.; Facchini, M. C.; Van Dingenen, R.; Ervens, B.; Nenes, A.; Nielsen, C. J.; Swietlicki, E.; Putaud, J. P.; Balkanski, Y.; Fuzzi, S.; Horth, J.; Moortgat, G. K.; Winterhalter, R.; Myhre, C. E. L.; Tsigaridis, K.; Vignati, E.; Stephanou, E. G.; Wilson, J. Organic Aerosol and Global Climate Modelling: A Review. *Atmos. Chem. Phys.* **2005**, *5*, 1053−1123.

(16) Russell, L. M.; Hawkins, L. N.; Frossard, A. A.; Quinn, P. K.; Bates, T. S. Carbohydrate-like Composition of Submicron Atmospheric Particles and their Production from Ocean Bubble Bursting. *Proc. Natl. Acad. Sci.* **2010**, *107*, 6652−6657.

(17) Frossard, A. A.; Russell, L. M.; Burrows, S. M.; Elliott, S. M.; Bates, T. S.; Quinn, P. K. Sources and Composition of Submicron Organic Mass in Marine Aerosol Particles. *J. Geophys. Res.: Atmos.* **2014**, *119*, 12977−13003.

(18) Fu, P. Q.; Kawamura, K.; Chen, J.; Charrière, B.; Sempéré, R. Organic Molecular Composition of Marine Aerosols over the Arctic Ocean in Summer: Contributions of Primary Emission and Secondary Aerosol Formation. *Biogeosciences* **2013**, *10*, 653−667.

(19) Scalabrin, E.; Zangrando, R.; Barbaro, E.; Kehrwald, N. M.; Gabrieli, J.; Barbante, C.; Gambaro, A. Amino Acids in Arctic Aerosols. *Atmos. Chem. Phys.* **2012**, *12*, 10453−10463.

(20) Fu, P.; Kawamura, K.; Chen, J.; Qin, M.; Ren, L.; Sun, Y.; Wang, Z.; Barrie, L. A.; Tachibana, E.; Ding, A.; Yamashita, Y. Fluorescent Water-Soluble Organic Aerosols in the High Arctic Atmosphere. *Sci. Rep.* **2015**, *5*, 9845.

(21) Hawkins, L. N.; Russell, L. Polysaccharides, Proteins, and Phytoplankton Fragments: Four Chemically Distinct Types of Marine Primary Organic Aerosol Classified by Single Particle Spectromicroscopy. *Adv. Meteorol.* **2010**, *2010*, 612132.

(22) Wilson, T. W.; Ladino, L. A.; Alpert, P. A.; Breckels, M. N.; Brooks, I. M.; Browse, J.; Burrows, S. M.; Carslaw, K. S.; Huffman, J. A.; Judd, C.; Kilthau, W. P.; Mason, R. H.; McFiggans, G.; Miller, L. A.; Nájera, J. J.; Polishchuk, E.; Rae, S.; Schiller, C. L.; Si, M.; Temprado, J. V.; Whale, T. F.; Wong, J. P. S.; Wurl, O.; Yakobi-Hancock, J. D.; Abbatt, J. P. D.; Aller, J. Y.; Bertram, A. K.; Knopf, D. A.; Murray, B. J. A Marine Biogenic Source of Atmospheric Ice-Nucleating Particles. *Nature* **2015**, *525*, 234−238.

(23) Bigg, E. K.; Leck, C. Properties of the Aerosol over the Central Arctic Ocean. *J. Geophys. Res.* **2001**, *106*, 32101−32109.

(24) Decesari, S.; Finessi, E.; Rinaldi, M.; Paglione, M.; Fuzzi, S.; Stephanou, E. G.; Tziaras, T.; Spyros, A.; Ceburnis, D.; O'Dowd, C.; Dall'Osto, M.; Harrison, R. M.; Allan, J.; Coe, H.; Facchini, M. C. Primary and Secondary Marine Organic Aerosols over the North Atlantic Ocean During the MAP experiment. *J. Geophys. Res.: Atmos.* **2011**, *116*, D22210.

(25) Eom, H. J.; Gupta, D.; Cho, H. R.; Hwang, H. J.; Hur, S. D.; Gim, Y.; Ro, C. U. Single-particle investigation of summertime and wintertime Antarctic sea spray aerosols using low-Z particle EPMA, Raman microspectrometry, and ATR-FTIR imaging techniques. *Atmos. Chem. Phys.* **2016**, *16*, 13823−13836.

(26) Lewis, S. L.; Saliba, G.; Russell, L. M.; Quinn, P. K.; Bates, T. S.; Behrenfeld, M. J. Seasonal Differences in Submicron Marine Aerosol Particle Organic Composition in the North Atlantic. *Front. Mar. Sci.* **2021**, *8*, 720208.
(27) Lawler, M. J.; Lewis, S. L.; Russell, L. M.; Quinn, P. K.; Bates, T. S.; Coffman, D. J.; Upchurch, L. M.; Saltzman, E. S. North Atlantic Marine Organic Aerosol Characterized by Novel Offline Thermal Desorption Mass Spectrometry: Polysaccharides, Recalcitrant Material, and Secondary Organics. *Atmos. Chem. Phys.* **2020**, *20*, 16007−16022.
(28) Kasparian, J.; Hassler, C.; Ibelings, B.; Berti, N.; Bigorre, S.; Djambazova, V.; Gascon-Diez, E.; Giuliani, G.; Houlmann, R.; Kiselev, D.; de Laborie, P.; Le, A.-D.; Magouroux, T.; Neri, T.; Palomino, D.; Pfändler, S.; Ray, N.; Sousa, G.; Staedler, D.; Tettamanti, F.; Wolf, J.-P.; Beniston, M. Assessing the Dynamics of Organic Aerosols over the North Atlantic Ocean. *Sci. Rep.* **2017**, *7*, 45476.
(29) Saliba, G.; Chen, C.-L.; Lewis, S.; Russell, L. M.; Quinn, P. K.; Bates, T. S.; Bell, T. G.; Lawler, M. J.; Saltzman, E. S.; Sanchez, K. J.; Moore, R.; Shook, M.; Rivellini, L.-H.; Lee, A.; Baetge, N.; Carlson, C. A.; Behrenfeld, M. J. Seasonal Differences and Variability of Concentrations, Chemical Composition, and Cloud Condensation Nuclei of Marine Aerosol Over the North Atlantic. *J. Geophys. Res.: Atmos.* **2020**, *125*, No. e2020JD033145.
(30) Quinn, P. K.; Bates, T. S.; Schulz, K. S.; Coffman, D. J.; Frossard, A. A.; Russell, L. M.; Keene, W. C.; Kieber, D. J. Contribution of Sea Surface Carbon Pool to Organic Matter Enrichment in Sea Spray Aerosol. *Nat. Geosci.* **2014**, *7*, 228−232.
(31) Park, J.; Dall'Osto, M.; Park, K.; Kim, J.-H.; Park, J.; Park, K.-T.; Hwang, C. Y.; Jang, G. I.; Gim, Y.; Kang, S.; Park, S.; Jin, Y. K.; Yum, S. S.; Simó, R.; Yoon, Y. J. Arctic Primary Aerosol Production Strongly Influenced by Riverine Organic Matter. *Environ. Sci. Technol.* **2019**, *53*, 8621−8630.
(32) May, N. W.; Gunsch, M. J.; Olson, N. E.; Bondy, A. L.; Kirpes, R. M.; Bertman, S. B.; China, S.; Laskin, A.; Hopke, P. K.; Ault, A. P.; Pratt, K. A. Unexpected Contributions of Sea Spray and Lake Spray Aerosol to Inland Particulate Matter. *Environ. Sci. Technol. Lett.* **2018**, *5*, 405−412.
(33) Zinke, J.; Salter, M. E.; Leck, C.; Lawler, M. J.; Porter, G. C. E.; Adams, M. P.; Brooks, I. M.; Murray, B. J.; Zieger, P. The development of a miniaturised balloon-borne cloud water sampler and its first deployment in the high Arctic. *Tellus B* **2021**, *73*, 1915614.
(34) Huang, Y. B.; Liu, X.; Laws, E. A.; Chen, B. Z.; Li, Y.; Xie, Y. Y.; Wu, Y. P.; Gao, K. S.; Huang, B. Q. Effects of increasing atmospheric CO2 on the marine phytoplankton and bacterial metabolism during a bloom: A coastal mesocosm study. *Sci. Total Environ.* **2018**, *633*, 618−629.
(35) Bertram, T. H.; Cochran, R. E.; Grassian, V. H.; Stone, E. A. Sea Spray Aerosol Chemical Composition: Elemental and Molecular Mimics for Laboratory Studies of Heterogeneous and Multiphase Reactions. *Chem. Soc. Rev.* **2018**, *47*, 2374−2400.
(36) Prather, K. A.; Hatch, C. D.; Grassian, V. H. Analysis of Atmospheric Aerosols. *Annu. Rev. Anal. Chem.* **2008**, *1*, 485−514.
(37) Saliba, G.; Sanchez, K. J.; Russell, L. M.; Twohy, C. H.; Roberts, G. C.; Lewis, S.; Dedrick, J.; McCluskey, C. S.; Moore, K.; DeMott, P. J.; Toohey, D. W. Organic Composition of Three Different Size Ranges of Aerosol Particles over the Southern Ocean. *Aerosol Sci. Technol.* **2021**, *55*, 268−288.
(38) Laskin, A.; Iedema, M. J.; Cowin, J. P. Quantitative Time-Resolved Monitoring of Nitrate Formation in Sea Salt Particles Using a CCSEM/EDX Single Particle Analysis. *Environ. Sci. Technol.* **2002**, *36*, 4948−4955.
(39) Laskin, A.; Iedema, M. J.; Ichkovich, A.; Graber, E. R.; Taraniuk, I.; Rudich, Y. Direct Observation of Completely Processed Calcium Carbonate Dust Particles. *Faraday Discuss.* **2005**, *130*, 453−468.
(40) DeMott, P. J.; Hill, T. C. J.; McCluskey, C. S.; Prather, K. A.; Collins, D. B.; Sullivan, R. C.; Ruppel, M. J.; Mason, R. H.; Irish, V. E.; Lee, T.; Hwang, C. Y.; Rhee, T. S.; Snider, J. R.; McMeeking, G. R.; Dhaniyala, S.; Lewis, E. R.; Wentzell, J. J. B.; Abbatt, J.; Lee, C.; Sultana, C. M.; Ault, A. P.; Axson, J. L.; Diaz Martinez, M.; Venero, I.; Santos-Figueroa, G.; Stokes, M. D.; Deane, G. B.; Mayol-Bracero, O. L.; Grassian, V. H.; Bertram, T. H.; Bertram, A. K.; Moffett, B. F.; Franc, G. D. Sea Spray Aerosol as a Unique Source of Ice Nucleating Particles. *Proc. Natl. Acad. Sci.* **2016**, *113*, 5797−5803.
(41) Prather, K. A.; Bertram, T. H.; Grassian, V. H.; Deane, G. B.; Stokes, M. D.; DeMott, P. J.; Aluwihare, L. I.; Palenik, B. P.; Azam, F.; Seinfeld, J. H.; Moffet, R. C.; Molina, M. J.; Cappa, C. D.; Geiger, F. M.; Roberts, G. C.; Russell, L. M.; Ault, A. P.; Baltrusaitis, J.; Collins, D. B.; Corrigan, C. E.; Cuadra-Rodriguez, L. A.; Ebben, C. J.; Forestieri, S. D.; Guasco, T. L.; Hersey, S. P.; Kim, M. J.; Lambert, W. F.; Modini, R. L.; Mui, W.; Pedler, B. E.; Ruppel, M. J.; Ryder, O. S.; Schoepp, N. G.; Sullivan, R. C.; Zhao, D. F. Bringing the Ocean into the Laboratory to Probe the Chemical Complexity of Sea Spray Aerosol. *Proc. Natl. Acad. Sci. U.S.A.* **2013**, *110*, 7550−7555.
(42) Bondy, A. L.; Wang, B.; Laskin, A.; Craig, R. L.; Nhliziyo, M. V.; Bertman, S. B.; Pratt, K. A.; Shepson, P. B.; Ault, A. P. Inland Sea Spray Aerosol Transport and Incomplete Chloride Depletion: Varying Degrees of Reactive Processing Observed during SOAS. *Environ. Sci. Technol.* **2017**, *51*, 9533−9542.
(43) Creamean, J. M.; Kirpes, R. M.; Pratt, K. A.; Spada, N. J.; Maahn, M.; de Boer, G.; Schnell, R. C.; China, S. Marine and Terrestrial Influences on Ice Nucleating Particles During Continuous Springtime Measurements in an Arctic Oilfield Location. *Atmos. Chem. Phys.* **2018**, *18*, 18023−18042.
(44) Gunsch, M. J.; Kirpes, R. M.; Kolesar, K. R.; Barrett, T. E.; China, S.; Sheesley, R. J.; Laskin, A.; Wiedensohler, A.; Tuch, T.; Pratt, K. A. Contributions of Transported Prudhoe Bay Oilfield Emissions to the Aerosol Population in Utqiaġvik, Alaska. *Atmos. Chem. Phys.* **2017**, *17*, 10879−10892.
(45) Kirpes, R.; Bondy, A.; Bonanno, D.; Moffet, R.; Wang, B.; Laskin, A.; Ault, A.; Pratt, K. Secondary Sulfate is Internally Mixed with Sea Spray Aerosol and Organic Aerosol in the Winter Arctic. *Atmos. Chem. Phys.* **2018**, *18*, 3937−3949.
(46) Kirpes, R. M.; Bonanno, D.; May, N. W.; Fraund, M.; Barget, A. J.; Moffet, R. C.; Ault, A. P.; Pratt, K. A. Wintertime Arctic Sea Spray Aerosol Composition Controlled by Sea Ice Lead Microbiology. *ACS Cent. Sci.* **2019**, *5*, 1760−1767.
(47) Hara, K.; Osada, K.; Nishita, K.; Yamagata, S.; Yamanocuhi, T.; Herber, A.; Matsunaga, K.; Iwasaka, Y.; Nagatani, M.; Nakata, H. Vertical Variations of Sea-salt Modification in the Boundary Layer of Spring Arctic During the ASTAR 2000 Campaign. *Tellus B* **2002**, *54*, 361−376.
(48) Deng, C.; Brooks, S. D.; Vidaurre, G.; Thornton, D. C. O. Using Raman Microspectroscopy to Determine Chemical Composition and Mixing State of Airborne Marine Aerosols over the Pacific Ocean. *Aerosol Sci. Technol.* **2014**, *48*, 193−206.
(49) Leaitch, W. R.; Russell, L. M.; Liu, J.; Kolonjari, F.; Toom, D.; Huang, L.; Sharma, S.; Chivulescu, A.; Veber, D.; Zhang, W. Organic functional groups in the submicron aerosol at 82.5° N, 62.5° W from 2012 to 2014. *Atmos. Chem. Phys.* **2018**, *18*, 3269−3287.
(50) Bates, T. S.; Quinn, P. K.; Frossard, A. A.; Russell, L. M.; Hakala, J.; Petäjä, T.; Kulmala, M.; Covert, D. S.; Cappa, C. D.; Li, S.-M.; Hayden, K. L.; Nuaaman, I.; McLaren, R.; Massoli, P.; Canagaratna, M. R.; Onasch, T. B.; Sueper, D.; Worsnop, D. R.; Keene, W. C. Measurements of Ocean Derived Aerosol off the Coast of California. *J. Geophys. Res.: Atmos.* **2012**, *117*, D00V15.
(51) Moffet, R. C.; Henn, T.; Laskin, A.; Gilles, M. K. Automated Chemical Analysis of Internally Mixed Aerosol Particles Using X-ray Spectromicroscopy at the Carbon K-Edge. *Anal. Chem.* **2010**, *82*, 7906−7914.
(52) Pham, D. Q.; O'Brien, R.; Fraund, M.; Bonanno, D.; Laskina, O.; Beall, C.; Moore, K. A.; Forestieri, S.; Wang, X. F.; Lee, C.; Sultana, C.; Grassian, V.; Cappa, C. D.; Prather, K. A.; Moffet, R. C. Biological Impacts on Carbon Speciation and Morphology of Sea Spray Aerosol. *ACS Earth Space Chem.* **2017**, *1*, 551−561.
(53) Schmitt-Kopplin, P.; Liger-Belair, G.; Koch, B. P.; Flerus, R.; Kattner, G.; Harir, M.; Kanawati, B.; Lucio, M.; Tziotis, D.; Hertkorn, N.; Gebefügi, I. Dissolved Organic Matter in Sea Spray: a Transfer Study from Marine Surface Water to Aerosols. *Biogeosciences* **2012**, *9*, 1571−1582.

(54) Riemer, N.; Ault, A. P.; West, M.; Craig, R. L.; Curtis, J. H. Aerosol Mixing State: Measurements, Modeling, and Impacts. *Rev. Geophys.* **2019**, *57*, 187−249.
(55) McNamara, S. M.; Kolesar, K. R.; Wang, S.; Kirpes, R. M.; May, N. W.; Gunsch, M. J.; Cook, R. D.; Fuentes, J. D.; Hornbrook, R. S.; Apel, E. C.; China, S.; Laskin, A.; Pratt, K. A. Observation of Road Salt Aerosol Driving Inland Wintertime Atmospheric Chlorine Chemistry. *ACS Cent. Sci.* **2020**, *6*, 684−694.
(56) Or, V. W.; Estillore, A. D.; Tivanski, A. V.; Grassian, V. H. Lab on a tip: atomic force microscopy - photothermal infrared spectroscopy of atmospherically relevant organic/inorganic aerosol particles in the nanometer to micrometer size range. *Analyst* **2018**, *143*, 2765−2774.
(57) Bondy, A. L.; Kirpes, R. M.; Merzel, R. L.; Pratt, K. A.; Banaszak Holl, M. M.; Ault, A. P. Atomic Force Microscopy-Infrared Spectroscopy of Individual Atmospheric Aerosol Particles: Subdiffraction Limit Vibrational Spectroscopy and Morphological Analysis. *Anal. Chem.* **2017**, *89*, 8594−8598.
(58) Kaluarachchi, C. P.; Or, V. W.; Lan, Y.; Madawala, C. K.; Hasenecz, E. S.; Crocker, D. R.; Morris, C. K.; Lee, H. D.; Mayer, K. J.; Sauer, J. S.; Lee, C.; Dorce, G.; Malfatti, F.; Stone, E. A.; Cappa, C. D.; Grassian, V. H.; Prather, K. A.; Tivanski, A. V. Size-Dependent Morphology, Composition, Phase State, and Water Uptake of Nascent Submicrometer Sea Spray Aerosols during a Phytoplankton Bloom. *ACS Earth Space Chem.* **2022**, *6*, 116−130.
(59) Lee, H. D.; Wigley, S.; Lee, C.; Or, V. W.; Hasenecz, E. S.; Stone, E. A.; Grassian, V. H.; Prather, K. A.; Tivanski, A. V. Physicochemical Mixing State of Sea Spray Aerosols: Morphologies Exhibit Size Dependence. *ACS Earth Space Chem.* **2020**, *4*, 1604−1611.
(60) Marcott, C.; Kansiz, M.; Dillon, E.; Cook, D.; Mang, M. N.; Noda, I. Two-Dimensional Correlation Analysis of Highly Spatially Resolved Simultaneous IR and Raman Spectral Imaging of Bioplastics Composite using Optical Photothermal Infrared and Raman Spectroscopy. *J. Mol. Struct.* **2020**, *1210*, 128045.
(61) Olson, N. E.; Xiao, Y.; Lei, Z.; Ault, A. P. Simultaneous Optical Photothermal Infrared (O-PTIR) and Raman Spectroscopy of Submicrometer Atmospheric Particles. *Anal. Chem.* **2020**, *92*, 9932−9939.
(62) Ault, A. P.; Peters, T. M.; Sawvel, E. J.; Casuccio, G. S.; Willis, R. D.; Norris, G. A.; Grassian, V. H. Single-Particle SEM-EDX Analysis of Iron-Containing Coarse Particulate Matter in an Urban Environment: Sources and Distribution of Iron within Cleveland, Ohio. *Environ. Sci. Technol.* **2012**, *46*, 4331−4339.
(63) May, N. W.; Olson, N. E.; Panas, M.; Axson, J. L.; Tirella, P. S.; Kirpes, R. M.; Craig, R. L.; Gunsch, M. J.; China, S.; Laskin, A.; Ault, A. P.; Pratt, K. A. Aerosol Emissions from Great Lakes Harmful Algal Blooms. *Environ. Sci. Technol.* **2018**, *52*, 397−405.
(64) Stokes, M. D.; Deane, G. B.; Prather, K.; Bertram, T. H.; Ruppel, M. J.; Ryder, O. S.; Brady, J. M.; Zhao, D. A Marine Aerosol Reference Tank System as a Breaking Wave Analogue for the Production of Foam and Sea-spray Aerosols. *Atmos. Meas. Tech.* **2013**, *6*, 1085−1094.
(65) Dickson, A. G.; Sabine, C. L.; Christian, J. R. SOP7 Determination of Dissolved Organic Carbon and Total Dissolved Nitrogen in Sea Water. *Guide to Best Practices for Ocean CO2 Measurements*; North Pacific Marine Science Organization, 2007; Vol. 3, pp 1−5.
(66) Hansell, D. A. Dissolved Organic Carbon Reference Material Program. *Eos. Trans. AGU* **2005**, *86*, 318.
(67) Brooks, I. M.; Yelland, M. J.; Upstill-Goddard, R. C.; Nightingale, P. D.; Archer, S.; d'Asaro, E.; Beale, R.; Beatty, C.; Blomquist, B.; Bloom, A. A.; Brooks, B. J.; Cluderay, J.; Coles, D.; Dacey, J.; DeGrandpre, M.; Dixon, J.; Drennan, W. M.; Gabriele, J.; Goldson, L.; Hardman-Mountford, N.; Hill, M. K.; Horn, M.; Hsueh, P.-C.; Huebert, B.; de Leeuw, G.; Leighton, T. G.; Liddicoat, M.; Lingard, J. J. N.; McNeil, C.; McQuaid, J. B.; Moat, B. I.; Moore, G.; Neill, C.; Norris, S. J.; O'Doherty, S.; Pascal, R. W.; Prytherch, J.; Rebozo, M.; Sahlee, E.; Salter, M.; Schuster, U.; Skjelvan, I.; Slagter, H.; Smith, M. H.; Smith, P. D.; Srokosz, M.; Stephens, J. A.; Taylor, P. K.; Telszewski, M.; Walsh, R.; Ward, B.; Woolf, D. K.; Young, D.; Zemmelink, H. Physical Exchanges at the Air-Sea Interface: UK-SOLAS Field Measurements. *Bull. Am. Meteorol. Soc.* **2009**, *90*, 629−644.
(68) Norris, S. J.; Brooks, I. M.; de Leeuw, G.; Sirevaag, A.; Leck, C.; Brooks, B. J.; Birch, C. E.; Tjernström, M. Measurements of Bubble Size Spectra Within Leads in the Arctic Summer Pack Ice. *Ocean Sci.* **2011**, *7*, 129−139.
(69) Phelps, A.; Ramble, D.; Leighton, T. The Use of a Combination Frequency Technique to Measure the Surf Zone Bubble Population. *J. Acoust. Soc. Am.* **1997**, *101*, 1981−1989.
(70) Phelps, A.; Leighton, T. Oceanic Bubble Population Measurements Using a Buoy-Deployed Combination Frequency Technique. *IEEE J. Oceanic Eng.* **1998**, *23*, 400−410.
(71) Deane, G. B.; Stokes, M. D. Air Entrainment Processes and Bubble Size Distributions in the Surf Zone. *J. Phys. Oceanogr.* **1999**, *29*, 1393−1403.
(72) May, N. W.; Axson, J. L.; Watson, A.; Pratt, K. A.; Ault, A. P. Lake Spray Aerosol Generation: a Method for Producing Representative Particles from Freshwater Wave Breaking. *Atmos. Meas. Tech.* **2016**, *9*, 4311−4325.
(73) Carey, W. M.; Fitzgerald, J. W.; Monahan, E. C.; Wang, Q. Measurement of the Sound Produced by a Tipping Trough with Fresh and Salt Water. *J. Acoust. Soc. Am.* **1993**, *93*, 3178−3192.
(74) Wang, Q.; Monahan, E. C. The Influence of Salinity on the Spectra of Bubbles Formed in Breaking Wave Simulations. *Sea Surface Sound*; World Scientific, 1995; Vol. *94*, pp 312−319
(75) Monahan, E. C. Comments on "Bubbles Produced by Breaking Waves in Fresh and Salt Water". *J. Phys. Oceanogr.* **2001**, *31*, 1931−1932.
(76) Cartmill, J. W.; Yang Su, M. Bubble Size Distribution Under Saltwater and Freshwater Breaking Waves. *Dynam. Atmos. Oceans* **1993**, *20*, 25−31.
(77) de Leeuw, G.; Moerman, M. M.; Cohen, L.; Brooks, B.; Smith, M.; Vignati, E. Aerosols, Bubbles and Sea Spray Production Studies During the RED Experiments. *12th Conference on Interaction of the Sea and Atmosphere of the American Meteorological Society*; American Meteorological Society: Long Beach, CA, 2003; pp 1−5.
(78) Laskina, O.; Morris, H. S.; Grandquist, J. R.; Estillore, A. D.; Stone, E. A.; Grassian, V. H.; Tivanski, A. V. Substrate-Deposited Sea Spray Aerosol Particles: Influence of Analytical Method, Substrate, and Storage Conditions on Particle Size, Phase, and Morphology. *Environ. Sci. Technol.* **2015**, *49*, 13447−13453.
(79) Hand, J. L.; Kreidenweis, S. M. A New Method for Retrieving Particle Refractive Index and Effective Density from Aerosol Size Distribution Data. *Aerosol Sci. Technol.* **2002**, *36*, 1012−1026.
(80) Khlystov, A.; Stanier, C.; Pandis, S. N. An Algorithm for Combining Electrical Mobility and Aerodynamic Size Distributions Data when Measuring Ambient Aerosol Special Issue ofAerosol Science and Technologyon Findings from the Fine Particulate Matter Supersites Program. *Aerosol Sci. Technol.* **2004**, *38*, 229−238.
(81) Pilson, M. E. Q. Chapter 4 Major Constituents of Seawater. In *An Introduction to the Chemistry of the Sea*, 2nd ed.; Cambridge University Press, 2013; pp 66−73.
(82) Laskin, A.; Wietsma, T. W.; Krueger, B. J.; Grassian, V. H. Heterogeneous Chemistry of Individual Mineral Dust Particles with Nitric Acid: A Combined CCSEM/EDX, ESEM, and ICP-MS Study. *J. Geophys. Res.: Atmos.* **2005**, *110*, D10208.
(83) Ault, A. P.; Guasco, T. L.; Baltrusaitis, J.; Ryder, O. S.; Trueblood, J. V.; Collins, D. B.; Ruppel, M. J.; Cuadra-Rodriguez, L. A.; Prather, K. A.; Grassian, V. H. Heterogeneous Reactivity of Nitric Acid with Nascent Sea Spray Aerosol: Large Differences Observed between and within Individual Particles. *J. Phys. Chem. Lett.* **2014**, *5*, 2493−2500.
(84) Axson, J. L.; May, N. W.; Colón-Bernal, I. D.; Pratt, K. A.; Ault, A. P. Lake Spray Aerosol: A Chemical Signature from Individual Ambient Particles. *Environ. Sci. Technol.* **2016**, *50*, 9835−9845.
(85) Shen, H.; Peters, T. M.; Casuccio, G. S.; Lersch, T. L.; West, R. R.; Kumar, A.; Kumar, N.; Ault, A. P. Elevated Concentrations of Lead in Particulate Matter on the Neighborhood-Scale in Delhi, India As Determined by Single Particle Analysis. *Environ. Sci. Technol.* **2016**, *50*, 4961−4970.

(86) Bondy, A. L.; Bonanno, D.; Moffet, R. C.; Wang, B.; Laskin, A.; Ault, A. P. The Diverse Chemical Mixing State of Aerosol Particles in the Southeastern United States. *Atmos. Chem. Phys.* **2018**, *18*, 12595−12612.
(87) Ault, A. P.; Zhao, D.; Ebben, C. J.; Tauber, M. J.; Geiger, F. M.; Prather, K. A.; Grassian, V. H. Raman Microspectroscopy and Vibrational Sum Frequency Generation Spectroscopy as Probes of the Bulk and Surface Compositions of Size-Resolved Sea Spray Aerosol Particles. *Phys. Chem. Chem. Phys.* **2013**, *15*, 6206−6214.
(88) Craig, R. L.; Bondy, A. L.; Ault, A. P. Computer-Controlled Raman Microspectroscopy (CC-Raman): A Method for the Rapid Characterization of Individual Atmospheric Aerosol Particles. *Aerosol Sci. Technol.* **2017**, *51*, 1099−1112.
(89) Bates, T. S.; Quinn, P. K.; Coffman, D. J.; Johnson, J. E.; Upchurch, L.; Saliba, G.; Lewis, S.; Graff, J.; Russell, L. M.; Behrenfeld, M. J. Variability in Marine Plankton Ecosystems Are Not Observed in Freshly Emitted Sea Spray Aerosol Over the North Atlantic Ocean. *Geophys. Res. Lett.* **2020**, *47*, No. e2019GL085938.
(90) Collins, D. B.; Ault, A. P.; Moffet, R. C.; Ruppel, M. J.; Cuadra-Rodriguez, L. A.; Guasco, T. L.; Corrigan, C. E.; Pedler, B. E.; Azam, F.; Aluwihare, L. I.; Bertram, T. H.; Roberts, G. C.; Grassian, V. H.; Prather, K. A. Impact of marine biogeochemistry on the chemical mixing state and cloud forming ability of nascent sea spray aerosol. *J. Geophys. Res.: Atmos.* **2013**, *118*, 8553−8565.
(91) Saliba, G.; Chen, C.-L.; Lewis, S.; Russell, L. M.; Rivellini, L.-H.; Lee, A. K. Y.; Quinn, P. K.; Bates, T. S.; Haëntjens, N.; Boss, E. S.; Karp-Boss, L.; Baetge, N.; Carlson, C. A.; Behrenfeld, M. J. Factors Driving the Seasonal and Hourly Variability of Sea-Spray Aerosol Number in the North Atlantic. *Proc. Natl. Acad. Sci.* **2019**, *116*, 20309−20314.
(92) Massey, F. J. The Kolmogorov-Smirnov Test for Goodness of Fit. *J. Am. Stat. Assoc.* **1951**, *46*, 68−78.
(93) Lilliefors, H. W. On the Kolmogorov-Smirnov test for Normality with Mean and Variance Unknown. *J. Am. Stat. Assoc.* **1967**, *62*, 399−402.
(94) Salter, M. E.; Nilsson, E. D.; Butcher, A.; Bilde, M. On the Seawater Temperature Dependence of the Sea Spray Aerosol Generated by a Continuous Plunging Jet. *J. Geophys. Res.: Atmos.* **2014**, *119*, 9052−9072.
(95) Salter, M. E.; Zieger, P.; Acosta Navarro, J. C.; Grythe, H.; Kirkevåg, A.; Rosati, B.; Riipinen, I.; Nilsson, E. D. An Empirically Derived Inorganic Sea Spray Source Function Incorporating Sea Surface Temperature. *Atmos. Chem. Phys.* **2015**, *15*, 11047−11066.
(96) Hultin, K.; Nilsson, E. D.; Krejci, R.; Mårtensson, E. M.; Ehn, M.; Hagström, Å.; de Leeuw, G. d. In situ Laboratory Sea Spray Production During the Marine Aerosol Production 2006 Cruise on the Northeastern Atlantic Ocean. *J. Geophys. Res.* **2010**, *115*, D06201.
(97) Laskin, A.; Moffet, R. C.; Gilles, M. K.; Fast, J. D.; Zaveri, R. A.; Wang, B.; Nigge, P.; Shutthanandan, J. Tropospheric Chemistry of Internally Mixed Sea Salt and Organic Particles: Surprising Reactivity of NaCl with Weak Organic Acids. *J. Geophys. Res.: Atmos.* **2012**, *117*, D15302.
(98) Schwier, A. N.; Sellegri, K.; Mas, S.; Charrière, B.; Pey, J.; Rose, C.; Temime-Roussel, B.; Jaffrezo, J. L.; Parin, D.; Picard, D.; Ribeiro, M.; Roberts, G.; Sempéré, R.; Marchand, N.; D'Anna, B. Primary Marine Aerosol Physical Flux and Chemical Composition During a Nutrient Enrichment Experiment in Mesocosms in the Mediterranean Sea. *Atmos. Chem. Phys.* **2017**, *17*, 14645−14660.
(99) Laskin, A.; Cowin, J. P.; Iedema, M. J. Analysis of Individual Environmental Particles Using Modern Methods of Electron Microscopy and X-ray Microanalysis. *J. Electron Spectrosc.* **2006**, *150*, 260−274.
(100) Forestieri, S. D.; Cornwell, G. C.; Helgestad, T. M.; Moore, K. A.; Lee, C.; Novak, G. A.; Sultana, C. M.; Wang, X.; Bertram, T. H.; Prather, K. A.; Cappa, C. D. Linking Variations in Sea Spray Aerosol Particle Hygroscopicity to Composition During Two Microcosm Experiments. *Atmos. Chem. Phys.* **2016**, *16*, 9003−9018.
(101) Guasco, T. L.; Cuadra-Rodriguez, L. A.; Pedler, B. E.; Ault, A. P.; Collins, D. B.; Zhao, D.; Kim, M. J.; Ruppel, M. J.; Wilson, S. C.; Pomeroy, R. S.; Grassian, V. H.; Azam, F.; Bertram, T. H.; Prather, K. A. Transition Metal Associations with Primary Biological Particles in Sea Spray Aerosol Generated in a Wave Channel. *Environ. Sci. Technol.* **2014**, *48*, 1324−1333.
(102) Salter, M. E.; Hamacher-Barth, E.; Leck, C.; Werner, J.; Johnson, C. M.; Riipinen, I.; Nilsson, E. D.; Zieger, P. Calcium Enrichment in Sea Spray Aerosol Particles. *Geophys. Res. Lett.* **2016**, *43*, 8277−8285.
(103) Wang, X. F.; Sultana, C. M.; Trueblood, J.; Hill, T. C. J.; Malfatti, F.; Lee, C.; Laskina, O.; Moore, K. A.; Beall, C. M.; McCluskey, C. S.; Cornwell, G. C.; Zhou, Y. Y.; Cox, J. L.; Pendergraft, M. A.; Santander, M. V.; Bertram, T. H.; Cappa, C. D.; Azam, F.; DeMott, P. J.; Grassian, V. H.; Prather, K. A. Microbial Control of Sea Spray Aerosol Composition: A Tale of Two Blooms. *ACS Cent. Sci.* **2015**, *1*, 124−131.
(104) Lee, C.; Sultana, C. M.; Collins, D. B.; Santander, M. V.; Axson, J. L.; Malfatti, F.; Cornwell, G. C.; Grandquist, J. R.; Deane, G. B.; Stokes, M. D.; Azam, F.; Grassian, V. H.; Prather, K. A. Advancing Model Systems for Fundamental Laboratory Studies of Sea Spray Aerosol Using the Microbial Loop. *J. Phys. Chem. A* **2015**, *119*, 8860−8870.
(105) Schwier, A. N.; Rose, C.; Asmi, E.; Ebling, A. M.; Landing, W. M.; Marro, S.; Pedrotti, M. L.; Sallon, A.; Iuculano, F.; Agusti, S.; Tsiola, A.; Pitta, P.; Louis, J.; Guieu, C.; Gazeau, F.; Sellegri, K. Primary marine aerosol emissions from the Mediterranean Sea during pre-bloom and oligotrophic conditions: correlations to seawater chlorophyll a from a mesocosm study. *Atmos. Chem. Phys.* **2015**, *15*, 7961−7976.
(106) Krueger, B. J.; Grassian, V. H.; Iedema, M. J.; Cowin, J. P.; Laskin, A. Probing heterogeneous chemistry of individual atmospheric particles using scanning electron microscopy and energy-dispersive X-ray analysis. *Anal. Chem.* **2003**, *75*, 5170−5179.
(107) Laskin, A.; Gaspar, D. J.; Wang, W.; Hunt, S. W.; Cowin, J. P.; Colson, S. D.; Finlayson-Pitts, B. J. Reactions at Interfaces As a Source of Sulfate Formation in Sea-Salt Particles. *Science* **2003**, *301*, 340−344.
(108) Hara, K.; Yamagata, S.; Yamanouchi, T.; Sato, K.; Herber, A.; Iwasaka, Y.; Nagatani, M.; Nakata, H. Mixing States of Individual Aerosol Particles in Spring Arctic Troposphere During ASTAR 2000 Campaign. *J. Geophys. Res.: Atmos.* **2003**, *108*, 4209.
(109) Larkin, P. J. IR and Raman Spectra−Structure Correlations: Characteristic Group Frequencies. In *Infrared and Raman Spectroscopy*; Larkin, P. J., Ed., 2nd ed.; Elsevier, 2018; Chapter 6, pp 85−134.
(110) Notingher, I.; Green, C.; Dyer, C.; Perkins, E.; Hopkins, N.; Lindsay, C.; Hench, L. L. Discrimination between ricin and sulphur mustard toxicity in vitro using Raman spectroscopy. *J. R. Soc., Interface* **2004**, *1*, 79−90.
(111) Almeida, M. R.; Alves, R. S.; Nascimbem, L. B. L. R.; Stephani, R.; Poppi, R. J.; de Oliveira, L. F. C. Determination of amylose content in starch using Raman spectroscopy and multivariate calibration analysis. *Anal. Bioanal. Chem.* **2010**, *397*, 2693−2701.
(112) Vasko, P.; Blackwell, J.; Koenig, J. L. Infrared and raman spectroscopy of carbohydrates. *Carbohydr. Res.* **1972**, *23*, 407−416.
(113) Cael, S. J.; Koenig, J. L.; Blackwell, J. Infrared and raman spectroscopy of carbohydrates. *Carbohydr. Res.* **1973**, *29*, 123−134.
(114) Mathlouthi, M.; Koenig, J. L. Vibrational Spectra of Carbohydrates. In *Advances in Carbohydrate Chemistry*; Tipson, R. S., Horton, D., Eds.; Academic Press, 1987; Vol. *44*, pp 7−89.
(115) Szarek, W. A.; Korppi-Tommola, S.-L.; Shurvell, H. F.; Smith, V. H., Jr; Martin, O. R. A Raman and infrared study of crystalline D-fructose, L-sorbose, and related carbohydrates. Hydrogen bonding and sweetness. *Can. J. Chem.* **1984**, *62*, 1512−1518.
(116) Wiercigroch, E.; Szafraniec, E.; Czamara, K.; Pacia, M.; Majzner, K.; Kochan, K.; Kaczor, A.; Baranska, M.; Malek, K. Raman and infrared spectroscopy of carbohydrates: A review. *Spectrochim. Acta, Part A* **2017**, *185*, 317.
(117) Kawamura, K.; Hoque, M. M. M.; Bates, T. S.; Quinn, P. K. Molecular distributions and isotopic compositions of organic aerosols over the western North Atlantic: Dicarboxylic acids, related compounds, sugars, and secondary organic aerosol tracers. *Org. Geochem.* **2017**, *113*, 229−238.

https://doi.org/10.1021/acsmeasuresciau.2c00041
ACS Meas. Sci. Au 2022, 2, 605−619

(118) Pakulski, J. D.; Benner, R. Abundance and distribution of carbohydrates in the ocean. *Limnol. Oceanogr.* **1994**, *39*, 930−940.
(119) Leck, C.; Gao, Q.; Mashayekhy Rad, F.; Nilsson, U. Size-resolved atmospheric particulate polysaccharides in the high summer Arctic. *Atmos. Chem. Phys.* **2013**, *13*, 12573−12588.
(120) Gao, F.; Han, L. J.; Liu, X. Vibration spectroscopic technique for species identification based on lipid characteristics. *Int. J. Agric. Biol. Eng.* **2017**, *10*, 255−268.
(121) McLaughlin, R. P.; Bird, B.; Reid, P. J. Vibrational analysis of isopropyl nitrate and isobutyl nitrate. *Spectrochim. Acta, Part A* **2002**, *58*, 2571−2580.
(122) Ovadnevaite, J.; Ceburnis, D.; Leinert, S.; Dall Osto, M.; Canagaratna, M. R.; O'Doherty, S. J.; Berresheim, H.; O'Dowd, C. D. Submicron NE Atlantic Marine Aerosol Chemical Composition and Abundance: Seasonal Trends and Air Mass Categorization. *J. Geophys. Res.* **2014**, *119*, 11,850−11,863.
(123) Tervahattu, H.; Juhanoja, J.; Kupiainen, K. Identification of an Organic Coating on Marine Aerosol Particles by TOF-SIMS. *J. Geophys. Res.* **2002**, *107*, ACH-18.
(124) Marty, J. C.; Saliot, A.; Buat-Ménard, P.; Chesselet, R.; Hunter, K. A. Relationship Between the Lipid Compositions of Marine Aerosols, the Sea Surface Microlayer, and Subsurface Water. *J. Geophys. Res.: Oceans* **1979**, *84*, 5707−5716.
(125) Ben Mabrouk, K.; Kauffmann, T. H.; Aroui, H.; Fontana, M. D. Raman Study of Cation Effect on Sulfate Vibration Modes in Solid State and in Aqueous Solutions. *J. Raman Spectrosc.* **2013**, *44*, 1603−1608.
(126) Kruus, P.; Hayes, A. C.; Adams, W. A. Determination of Ratios of Sulfate to Bisulfate Ions in Aqueous Solutions by Raman Spectroscopy. *J. Solution Chem.* **1985**, *14*, 117−128.
(127) Wang, A.; Freeman, J.; Jolliff, B.; Chou, I. M. Sulfates on Mars: A Systematic Raman Spectroscopic Study of Hydration States of Magnesium Sulfates. *Geochim. Cosmochim. Acta* **2006**, *70*, 6118−6135.
(128) Chi, J. W.; Li, W. J.; Zhang, D. Z.; Zhang, J. C.; Lin, Y. T.; Shen, X. J.; Sun, J. Y.; Chen, J. M.; Zhang, X. Y.; Zhang, Y. M.; Wang, W. X. Sea Salt Aerosols as a Reactive Surface for Inorganic and Organic Acidic Gases in the Arctic Troposphere. *Atmos. Chem. Phys.* **2015**, *15*, 11341−11353.
(129) Kirpes, R. M.; Rodriguez, B.; Kim, S.; China, S.; Laskin, A.; Park, K.; Jung, J.; Ault, A. P.; Pratt, K. A. Emerging Investigator Series: Influence of Marine Emissions and Atmospheric Processing on Individual Particle Composition of Summertime Arctic Aerosol over the Bering Strait and Chukchi Sea. *Environ. Sci.: Processes Impacts* **2020**, *22*, 1201−1213.
(130) Hopkins, R. J.; Desyaterik, Y.; Tivanski, A. V.; Zaveri, R. A.; Berkowitz, C. M.; Tyliszczak, T.; Gilles, M. K.; Laskin, A. Chemical Speciation of Sulfur in Marine Cloud Droplets and Particles: Analysis of Individual Particles from the Marine Boundary Layer over the California Current. *J. Geophys. Res.: Atmos.* **2008**, *113*, D04209.
(131) McInnes, L. M.; Covert, D. C.; Quinn, P. K.; Germani, M. S. Measurements of Chloride Depletion and Sulfur Enrichment in Individual Sea-Salt Particles Collected from the Remote Marine Boundary Layer. *J. Geophys. Res.: Atmos.* **1994**, *99*, 8257−8268.
(132) de Aza, P. N.; Santos, C.; Pazo, A.; de Aza, S.; Cuscó, R.; Artús, L. Vibrational Properties of Calcium Phosphate Compounds. 1. Raman Spectrum of β-Tricalcium Phosphate. *Chem. Mater.* **1997**, *9*, 912−915.
(133) Leung, Y.; Anton Walters, M.; Blumenthal, N. C.; Ricci, J. L.; Spivak, J. M. Determination of the Mineral Phases and Structure of the Bone-Implant Interface Using Raman Spectroscopy. *J. Biomed. Mater. Res.* **1995**, *29*, 591−594.
(134) Dufresne, W. J. B.; Rufledt, C. J.; Marshall, C. P. Raman Spectroscopy of the Eight Natural Carbonate Minerals of Calcite Structure. *J. Raman Spectrosc.* **2018**, *49*, 1999−2007.
(135) Venkateswarlu, P.; Bist, H. D.; Jain, Y. S. Laser Excited Raman Spectrum of Ammonium Sulfate Single Crystal. *J. Raman Spectrosc.* **1975**, *3*, 143−151.
(136) Kaczor, A.; Baranska, M. Structural Changes of Carotenoid Astaxanthin in a Single Algal Cell Monitored in situ by Raman Spectroscopy. *Anal. Chem.* **2011**, *83*, 7763−7770.
(137) Subramanian, B.; Tchoukanova, N.; Djaoued, Y.; Pelletier, C.; Ferron, M.; Robichaud, J. Investigations on the Geometrical Isomers of Astaxanthin: Raman Spectroscopy of Conjugated Polyene Chain with Electronic and Mechanical Confinement. *J. Raman Spectrosc.* **2014**, *45*, 299−304.
(138) Brizuela, A. B.; Bichara, L. C.; Romano, E.; Yurquina, A.; Locatelli, S.; Brandán, S. A. A Complete Characterization of the Vibrational Spectra of Sucrose. *Carbohydr. Res.* **2012**, *361*, 212−218.
(139) Lu, Q.; Zografi, G. Properties of Citric Acid at the Glass Transition. *J. Pharm. Sci.* **1997**, *86*, 1374−1378.
(140) Bellisola, G.; Sorio, C. Infrared Spectroscopy and Microscopy in Cancer Research and Diagnosis. *Am. J. Cancer Res.* **2012**, *2*, 1−21.
(141) Jang, M.; Kamens, R. M. Atmospheric Secondary Aerosol Formation by Heterogeneous Reactions of Aldehydes in the Presence of a Sulfuric Acid Aerosol Catalyst. *Environ. Sci. Technol.* **2001**, *35*, 4758−4766.
(142) Coury, C.; Dillner, A. A Method to Quantify Organic Functional Groups and Inorganic Compounds in Ambient Aerosols Using Attenuated Total Reflectance FTIR Spectroscopy and Multivariate Chemometric Techniques. *Atmos. Environ.* **2008**, *42*, 5923−5932.
(143) Stone, N.; Kendall, C.; Shepherd, N.; Crow, P.; Barr, H. Near-Infrared Raman Spectroscopy for the Classification of Epithelial Pre-cancers and Cancers. *J. Raman Spectrosc.* **2002**, *33*, 564−573.
(144) Bitar, R.; Martinho, H.; Tierra-Criollo, C. J.; Zambelli Ramalho, L.; Netto, M.; Martin, A. Biochemical Analysis of Human Breast Tissues Using Fourier-Transform Raman Spectroscopy. *J. Biomed. Opt.* **2006**, *11*, 054001.
(145) Ruggeri, G.; Takahama, S. Technical Note: Development of Chemoinformatic Tools to Enumerate Functional Groups in Molecules for Organic Aerosol Characterization. *Atmos. Chem. Phys.* **2016**, *16*, 4401−4422.
(146) Guillén, M. D.; Cabo, N. Infrared Spectroscopy in the Study of Edible Oils and Fats. *J. Sci. Food Agric.* **1997**, *75*, 1−11.
(147) Wells, H. A.; Atalla, R. H. An Investigation of the Vibrational Spectra of Glucose, Galactose and Mannose. *J. Mol. Struct.* **1990**, *224*, 385−424.
(148) Popovicheva, O.; Kireeva, E.; Shonija, N.; Vojtisek-Lom, M.; Schwarz, J. FTIR Analysis of Surface Functionalities on Particulate Matter Produced by Off-Road Diesel Engines Operating on Diesel and Biofuel. *Environ. Sci. Pollut. Res.* **2014**, *22*, 4534−4544.
(149) Marchessault, R. H.; Liang, C. Y. Infrared Spectra of Crystalline Polysaccharides. III. Mercerized Cellulose. *J. Polym. Sci.* **1960**, *43*, 71−84.
(150) Allen, D. T.; Palen, E. J.; Haimov, M. I.; Hering, S. V.; Young, J. R. Fourier Transform Infrared Spectroscopy of Aerosol Collected in a Low Pressure Impactor (LPI/FTIR): Method Development and Field Calibration. *Aerosol Sci. Technol.* **1994**, *21*, 325−342.
(151) Jang, M.; Carroll, B.; Chandramouli, B.; Kamens, R. M. Particle Growth by Acid-Catalyzed Heterogeneous Reactions of Organic Carbonyls on Preexisting Aerosols. *Environ. Sci. Technol.* **2003**, *37*, 3828−3837.
(152) Liu, Y.; Yang, Z.; Desyaterik, Y.; Gassman, P. L.; Wang, H.; Laskin, A. Hygroscopic Behavior of Substrate-Deposited Particles Studied by micro-FT-IR Spectroscopy and Complementary Methods of Particle Analysis. *Anal. Chem.* **2008**, *80*, 633−642.
(153) Ovalles, J.; Gallignani, M.; Rondón, R.; Brunetto, M. R.; Luna, R. Determination of Sulphate for Measuring Magnesium Sulphate in Pharmaceuticals by Flow Analysis-Fourier Transforms Infrared Spectroscopy. *Lat. Am. J. Pharm.* **2009**, *28*, 173−182.
(154) Liu, Y.; Wang, A.; Freemen, J. Raman, MIR, and NIR Spectroscopic Study of Calcium Sulfates: Gypsum, Bassanite, and Anhydrite. *40th Lunar and Planetary Science Conference*; Lunar and Planetary Institute, 2009; p 2128.
(155) Onasch, T.; Siefert, R.; Brooks, S.; Prenni, A.; Murray, B.; Wilson, M.; Tolbert, M. Infrared Spectroscopic Study of the Deliquescence and Efflorescence of Ammonium Sulfate Aerosol as a Function of Temperature. *J. Geophys. Res.* **1999**, *104*, 21317−21326.

https://doi.org/10.1021/acsmeasuresciau.2c00041
ACS Meas. Sci. Au 2022, 2, 605−619

(156) Ferraro, J. R. Inorganic infrared spectroscopy. *J. Chem. Educ.* **1961**, *38*, 201−208.
(157) Klähn, M.; Mathias, G.; Kötting, C.; Nonella, M.; Schlitter, J.; Gerwert, K.; Tavan, P. IR Spectra of Phosphate Ions in Aqueous Solution: Predictions of a DFT/MM Approach Compared with Observations. *J. Phys. Chem. A* **2004**, *108*, 6186−6194.
(158) Nash, K. L.; Jessica Sully, K.; Horn, A. B. Infrared spectroscopic studies of the low temperature interconversion of sulfuric acid hydrates. *Phys. Chem. Chem. Phys.* **2000**, *2*, 4933−4940.
(159) Krost, K. J.; McClenny, W. A. FT-IR Transmission Spectroscopy for Quantitation of Ammonium Bisulfate in Fine-Particulate Matter Collected on Teflon Filters. *Appl. Spectrosc.* **1994**, *48*, 702−705.
(160) Kunimatsu, K.; Samant, M. G.; Seki, H. In-situ FT-IR Spectroscopic Study of Bisulfate and Slfate Adsorption on a Platinum Electrode: Part 2. Mildly Acid and Alkaline Sodium Sulfate Solutions. *J. Electroanal. Chem. Interfacial Electrochem.* **1989**, *272*, 185−194.
(161) Théorêt, A.; Sandorfy, C. Infrared Spectra and Crystalline Phase Transitions of Ammonium Nitrate. *Can. J. Chem.* **1964**, *42*, 57−62.
(162) Ramseyer, K.; Miano, T. M.; D'Orazio, V.; Wildberger, A.; Wagner, T.; Geister, J. Nature and Origin of Organic Matter in Carbonates From Speleothems, Marine Cements and Coral Skeletons. *Org. Geochem.* **1997**, *26*, 361−378.
(163) Krimm, S.; Bandekar, J. Vibrational Spectroscopy and Conformation of Peptides, Polypeptides, and Proteins. *Advances in Protein Chemistry*; Anfinsen, C. B., Edsall, J. T., Richards, F. M., Eds.; Academic Press, 1986; Vol. *38*, pp 181−364.
(164) Barth, A.; Zscherp, C. What Vibrations Tell about Proteins. *Q. Rev. Biophys.* **2002**, *35*, 369−430.
(165) Balch, W. M.; Drapeau, D. T.; Bowler, B. C.; Record, N. R.; Bates, N. R.; Pinkham, S.; Garley, R.; Mitchell, C. Changing Hydrographic, Biogeochemical, and Acidification Properties in the Gulf of Maine as Measured by the Gulf of Maine North Atlantic Time Series, GNATS, Between 1998 and 2018. *J. Geophys. Res.: Biogeosci.* **2022**, *127*, No. e2022JG006790.
(166) Forestieri, S. D.; Moore, K. A.; Martinez Borrero, R.; Wang, A.; Stokes, M. D.; Cappa, C. D. Temperature and Composition Dependence of Sea Spray Aerosol Production. *Geophys. Res. Lett.* **2018**, *45*, 7218−7225.

https://doi.org/10.1021/acsmeasuresciau.2c00041
ACS Meas. Sci. Au 2022, 2, 605−619